DISSERTATIONES
PHYSICAE
UNIVERSITATIS
TARTUENSIS
**128**

HEIDO TROFIMOV

# Polluted clouds at air pollution hot spots help to better understand anthropogenic impacts on Earth's climate

DISSERTATIONES PHYSICAE UNIVERSITATIS TARTUENSIS
**128**

DISSERTATIONES PHYSICAE UNIVERSITATIS TARTUENSIS
**128**

**HEIDO TROFIMOV**

# Polluted clouds at air pollution hot spots help to better understand anthropogenic impacts on Earth's climate

UNIVERSITY OF TARTU
Press
1632

This study was carried out at the University of Tartu, Institute of Physics.

The Dissertation was admitted on June 8, 2022, in partial fulfillment of the requirements for the degree of Doctor of Philosophy in Physics, and allowed for defense by the Council of the Institute of Physics, University of Tartu.

Supervisors: Velle Toll, PhD, Associate Professor in Atmospheric Physics, Laboratory of Atmospheric Physics, Institute of Physics, University of Tartu, Estonia

Piia Post, PhD, Associate Professor in Meteorology and Climatology, Head of Laboratory, Laboratory of Atmospheric Physics, Institute of Physics, University of Tartu, Estonia

Opponent: Risto Makkonen, Research Professor, Finnish Meteorological Institute, Finland

Defense: August 25, 2022

Publication of this thesis is granted by the Institute of Ecology and Earth Sciences, University of Tartu and by the University of Tartu ASTRA Project PER ASPERA Doctoral School of Earth Sciences and Ecology (2014-2020.4.01.16-0027), created under the auspices of the European Regional Development Fund.


ISSN 1406-0647
ISBN 978-9949-03-955-5 (print)
ISBN 978-9949-03-956-2 (pdf)



University of Tartu Press
www.tyk.ee

# CONTENTS

# LIST OF ORIGINAL PUBLICATIONS

This thesis is based on the following publications, which are referred to in the text by their Roman numerals.

**I** Trofimov, H., Bellouin, N. and Toll, V.: Large-scale industrial cloud perturbations confirm bidirectional cloud water responses to anthropogenic aerosols. Journal of Geophysical Research: Atmospheres, 125(14), doi:10.1029/2020JD032575, 2020.

**II** Trofimov, H., Post, P., Gryspeerdt, E. and Toll, V.: Meteorological Conditions Favorable for Strong Anthropogenic Aerosol Impacts on Clouds. Journal of Geophysical Research: Atmospheres, 127(4), doi:10.1029/2021JD035871, 2022.

**III** Rahu, J., Trofimov, H., Post, P. and Toll, V.: Diurnal Evolution of Cloud Water Responses to Aerosols, Journal of Geophysical Research: Atmospheres, 127(10), doi: 10.1029/2021JD035091, 2022.

## Author's contributions

**I** Identification of the polluted cloud areas in the satellite images and analysis of the observations. Preparing most of the manuscript.

**II** Part of the study design. Carrying out all the analysis. Preparing most of the manuscript.

**III** Analysis of the MODIS satellite data. Contributing to the manuscript.

# ABSTRACT

The impact of air pollution particles, i.e aerosols, on clouds is the most uncertain mechanism of anthropogenic climate forcing. It is especially uncertain what happens to cloud thickness, coverage and lifetime when additional aerosols, on which water vapour condenses, are added to clouds due to anthropogenic activities, and more numerous smaller cloud droplets are formed. We can answer these questions by comparing the properties of polluted clouds at air pollution hot spots to nearby unpolluted clouds. Here, we show that large-scale polluted cloud areas, which cover hundreds by hundreds of kilometres, exist around the world. Large-scale anthropogenic cloud perturbations behave similarly to smaller-scale ship-track-like polluted cloud tracks, and cloud water response to anthropogenic aerosols is weak on average. Strong anthropogenic cloud perturbations occur intermittently and only in the case of favourable meteorological conditions. Our results help to better quantify the aerosol radiative forcing and will ultimately lead to more reliable climate projections.

# 1. INTRODUCTION

## 1.1 Aerosol forcing of Earth's climate

Aerosols, fine solid and liquid particles suspended in the atmosphere, exercise a major impact on Earth's climate, smaller but comparable to the impact of anthropogenic greenhouse gases. The net effect of anthropogenic aerosols on climate is cooling, but the extent to which it offsets the warming effect of greenhouse gases is still very uncertain (Bellouin et al., 2020). Both greenhouse gases and aerosols alter Earth's energy budget at the top of the atmosphere, which in turn triggers climate system responses. Such perturbations in the energy budget are called radiative forcings. Other anthropogenic radiative forcings result e.g., from land surface changes and ozone depletion. Variability in solar irradiance is an example of natural radiative forcing. Effective radiative forcing (ERF) is a measure of energy imbalance after atmospheric temperatures, water vapor and clouds have been allowed to adjust to the forcing (Myhre et al., 2013). The total anthropogenic ERF over the industrial period 1750-2019 is +2.72 ($\pm$0.76) W/m$^2$ according to the 6th Intergovernmental Panel on Climate Change (IPCC) assessment report (Forster et al., 2021). Positive forcing means that more energy is trapped within the atmosphere, which leads to a warming effect. Anthropogenic emissions of greenhouse gases contribute +3.84 ($\pm$0.38) W/m$^2$ to the total ERF, while the impact of anthropogenic aerosols is -1.3 ($\pm$0.7) W/m$^2$ (Forster et al., 2021). The uncertainty associated with the cooling effect of aerosols is therefore nearly two times larger than the uncertainty of the warming effect from greenhouse gases. This means that the uncertainty associated with the cooling effect of aerosols dominates the uncertainty of the total anthropogenic climate forcing.

Aerosols have both direct and indirect impacts on Earth's energy budget. The direct effect concerns the absorption and scattering of both shortwave and longwave radiation by aerosol particles (Bellouin et al., 2005). Here, the exact radiative response depends on the aerosol type, but the overall direct radiative effect of aerosols is negative forcing, which is in the magnitude of -0.3 ($\pm$0.3) W/m$^2$ (Forster et al., 2021).

The rest of aerosol forcing comes from aerosol-cloud interactions, which is the most poorly understood mechanism of anthropogenic climate forcing. Forcing by aerosol-cloud interactions is estimated to be -1.0 ($\pm$0.7) W/m$^2$ (Forster et al., 2021). Aerosols modulate cloud properties by acting as cloud condensation nuclei on which water vapour condenses, which leads to a variety of indirect aerosol effects on Earth's climate. Twomey effect or cloud brightening is a well-understood indirect effect that contributes to negative forcing: aerosols raise the cloud albedo by increasing cloud droplet number concentration (CDNC) and decreasing the size of cloud droplets (Twomey et al., 1974). Other aerosol indirect effects concern the changes in cloud thickness, cloud coverage, and lifetime (e.g. Albrecht, 1989), which in turn can further

modulate cloud albedo and in some cases lead to overall positive forcing (Forster et al., 2021), despite the brightening which comes from Twomey effect. If, however, these further indirect effects substantially add to the initial negative forcing that comes from the Twomey effect, then aerosol can have a very strong cooling effect on the climate. Each scenario leads to a drastically different future climate for a given scenario of greenhouse gas and aerosol emissions, and strong present-day aerosol forcing would mean that strong future warming is expected (Andrae et al., 2005, Stevens et al., 2016).

Uncertainty in aerosol radiative forcing also hinders improvements in estimates of climate sensitivity and transfers into uncertainty in the global warming level that results from rising levels of greenhouse gases (Stevens et al., 2016). If the anthropogenic radiative forcing was known more accurately, we could better estimate the climate sensitivity for projecting future climate based on the observational record (Bellouin et al., 2020). As reliable climate projections are needed for policy- and decision-making for climate change mitigation and adaptation, better constraining the anthropogenic aerosol forcing of Earth's climate is of great importance.

## 1.2 Research goals

In liquid-phase clouds, the cloud brightening through the Twomey effect can lead to the emergence of so-called pollution tracks (Fig. 1, 2), quasi-linear polluted cloud lines, which are detectable from satellite images in the near-infrared (NIR) spectral region. Such tracks were first spotted as trails from the ships and for that reason were named "ship tracks" (Coakley et al., 1987). Pollution tracks occur more easily over oceans, where the air is less polluted and clouds are therefore more susceptible to aerosol pollution. However, pollution tracks are detectable also over land, especially if there is an isolated pollution source in an otherwise pristine area, where polluted cloud tracks can stand out against the background of non-polluted clouds with larger droplets (Toll et al., 2019).

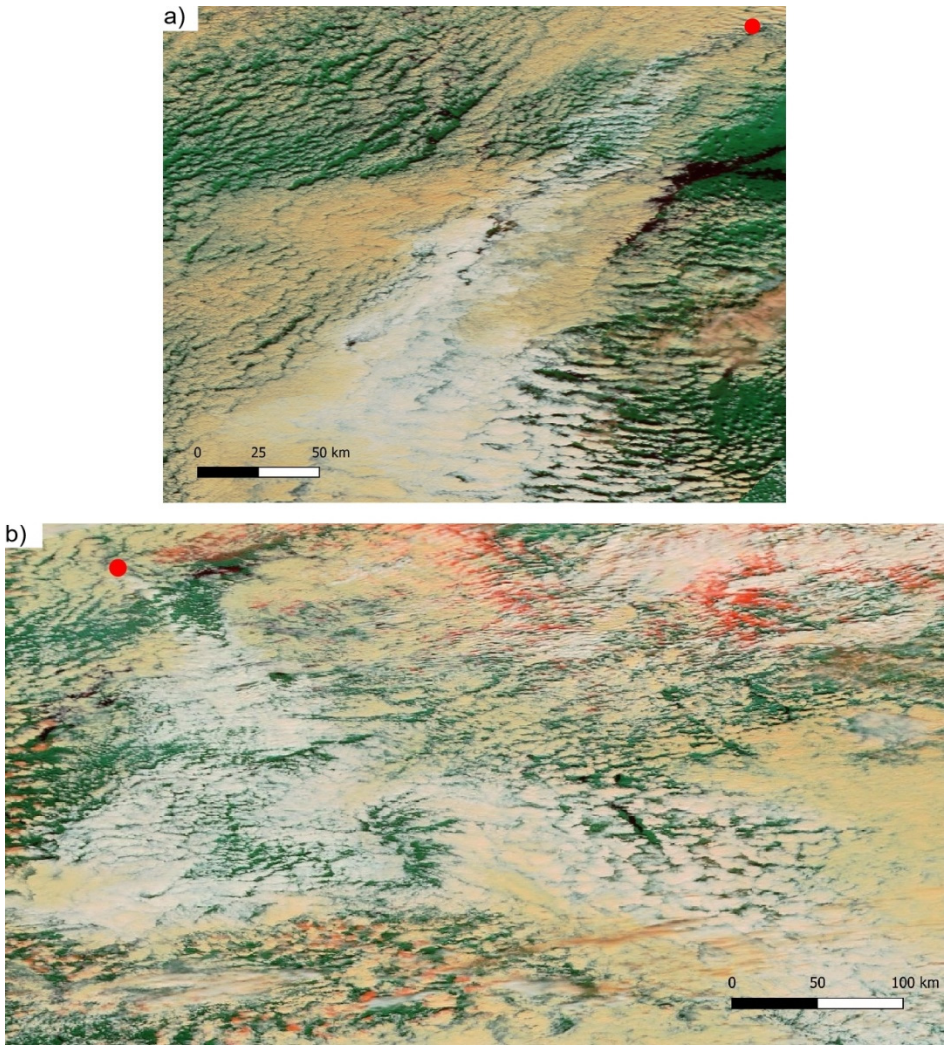


**Figure 1**. Example MODIS images of polluted clouds near Norilsk. In these composite images, polluted clouds appear in in grey-white colors, while unpolluted clouds appear in yellow-brown colors. Green color signifies vegetation and red color indicates the presence of ice or snow. The location of Norilsk factories is marked with a red dot. Image (a) was taken on August 26, 2006 and image (b) was taken on June 27, 2000 [I].

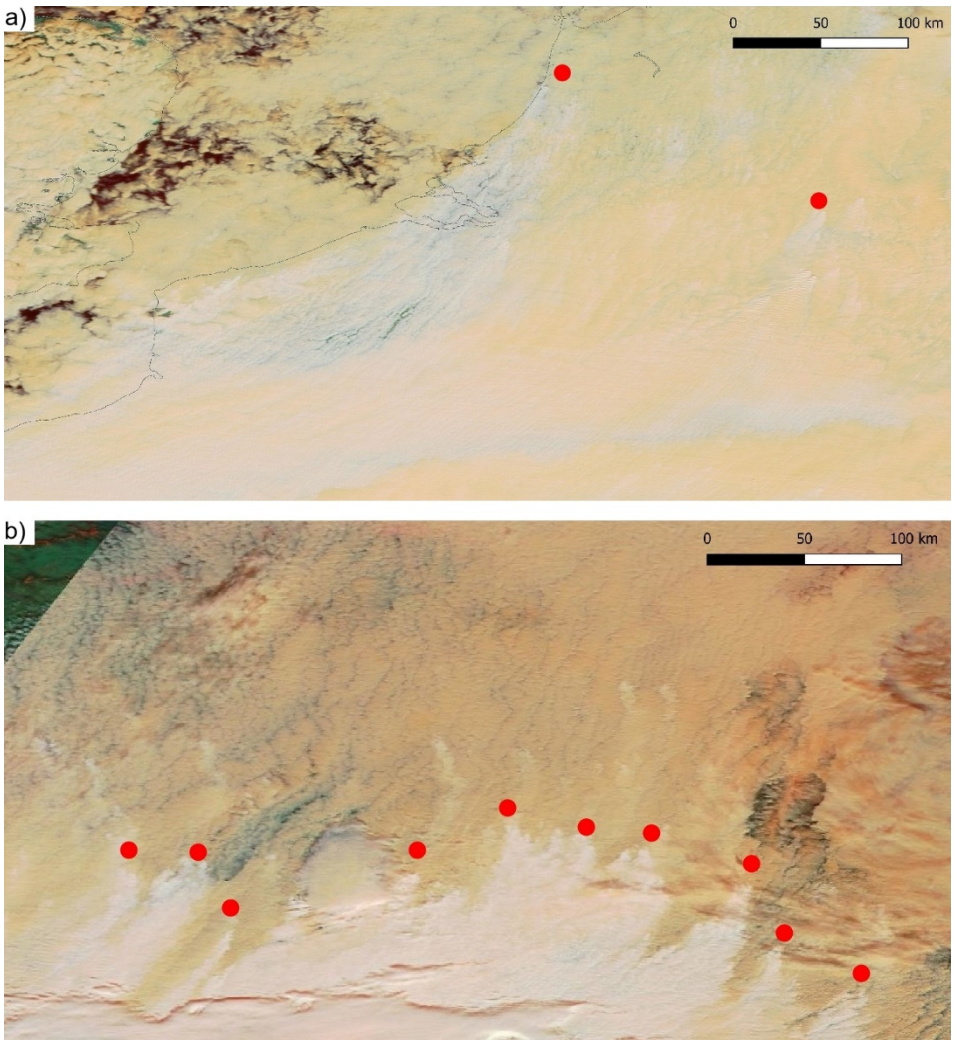


**Figure 2.** Examples of non-Norilsk large-scale polluted clouds. In these MODIS composite images, polluted clouds appear in grey-white colors and unpolluted clouds in yellow-brown colors. The approximate locations of aerosol sources are marked with red dots. Image (a) shows pollution downwind of urban and industrial sources in Europe, March 19, 2016 and image (b) shows clouds polluted by wildfire smoke in Russia, September 30, 2016 [I].

The major advantage of studying these perturbations is the possibility to directly compare the properties of polluted clouds to the nearby unpolluted clouds with certainty in the causality of the observed changes, thereby overcoming the limits of merely correlative studies (Toll et al., 2019). However, we do not know how well the pollution tracks represent the global aerosol effect. Aerosols

can have an impact on the radiative properties of clouds without forming visible tracks, and this impact may be different from that of tracks alone (Possner et al., 2018; Glassmeier et al., 2021). Weak tracks often go undetected and tracks are too small to be included directly in climate models (Yuan et al., 2019).

Toll et al. (2019), using observational evidence from pollution tracks, invalidated the common postulation that aerosols initiate only a strong increase of cloud water amount in polluted clouds. However, the average width of studied pollution tracks was only tens of kilometres, leaving open the question of the representativeness of the results. This dissertation aims to tackle the question of polluted cloud tracks' representativeness of the global average cloud responses to aerosols. To evaluate the global representativeness, we:

1) study large-scale cloud perturbations similar to pollution tracks to tell if the cloud responses in large-scale perturbations are similar to small-scale tracks (study [I]);
2) study the occurrence frequency and meteorological conditions favourable for pollution track formation (study [II]).

## 1.3 Theses

- Satellite observations confirm aerosol-induced decreases in cloud droplet size in large areas compared to nearby less polluted areas [I].
- Aerosol-induced cloud water increases and decreases compensate each other at large spatial scales, similarly to ship-track-like perturbations [I].
- On average, the Twomey effect is more important than the effect of cloud water changes for the aerosol radiative forcing of the Earth's climate [I].
- Strong perturbations tend to form in less polluted and thin clouds under stable and dry conditions [II].
- Strong continental anthropogenic cloud perturbations occur on 20 to 37 % of days with liquid-phase clouds [II].
- Large-scale atmospheric circulation largely determines the occurrence of conditions favouring the formation of polluted cloud tracks [II].

# 2. METHODS

## 2.1 Detection of pollution tracks

Pollution tracks can be detected due to their elevated near-infrared reflectance, as described by the Twomey effect (Twomey et al., 1974, Toll et al., 2017). We searched for pollution tracks visually by examining composite Terra Moderate Resolution Imaging Spectroradiometer (MODIS) satellite images. The composition of MODIS channels 3, 6 and 7 (corresponding to wavelengths 0.459–0.479 μm, 1.628–1.652 μm, and 2.105–2.155 μm) creates suitable images for the visual detection of tracks [I-II]. MODIS is on board the Terra and Aqua satellites, launched respectively in 1999 and 2002.

We sampled pollution tracks mainly for three sites, where we had determined beforehand that tracks form frequently enough to collect enough data, although tracks from various other regions were also analysed (Fig. 3). The three main sites were Norilsk and Cherepovets in Russia and Thompson in Canada. In these locations, there is an isolated pollution source in an otherwise unpolluted environment. The sulfur dioxide (SO2) emissions from Norilsk have been estimated to be over 2 Mt per year by Carn et al. (2004), which is about 2% of global anthropogenic SO2 emissions (Smith et al., 2011). This makes Norilsk an extraordinarily strong localised source of SO2. The polluted cloud tracks originating from the Norilsk factory are often very large, covering hundreds by hundreds of kilometres.

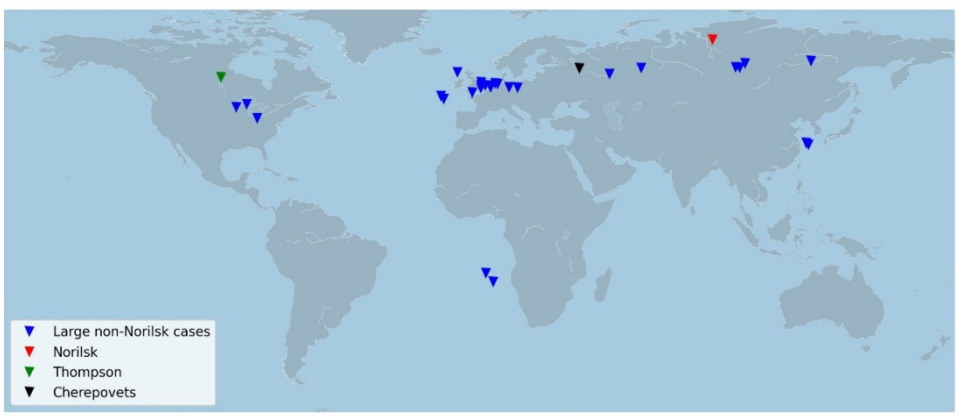


**Figure 3**. The locations of analysed polluted clouds (adapted from [I]).

Besides Norilsk, there are other isolated pollution sources around which pollution tracks regularly form, although in general, these tracks are not as large as they are in Norilsk. In Thompson, as in Norilsk, emissions from the smelting and concentrating of nickel cause pollution tracks. In Cherepovets, iron and

steel production processes are the primary pollution source (Table 1). Besides Norilsk, we found individual examples of large-scale tracks worldwide, including major industrial regions in Europe, Eastern United States, and Eastern Asia (Fig. 3).

**Table 1.** The three main pollution hot spots used for the analysis [II].

| Site of study | Coordinates | Elevation above sea level | The main source of air pollution |
|---|---|---|---|
| **Norilsk** | 69.33°N, 88.22°E | 90 m | The smelting and concentrating of nickel |
| **Thompson** | 55.74°N, 97.85°W | 224 m | The smelting and concentrating of nickel |
| **Cherepovets** | 59.12°N, 37.9°E | 130 m | Processes of iron and steel production |

The MODIS instrument can be used to get snapshots of clouds during various times of the day, depending on the geographical location [III]. These various times can be converted to a normalised time coordinate, where 0 is the local sunrise, 0.5 is the local noon, and 1 is the local sunset. In this way, we studied the diurnal evolution of cloud responses to aerosols, using MODIS data from Toll et al. 2019 [III]. However, MODIS data can give only the average temporal characteristics of multiple different pollution tracks, and it can't be used to study the temporal evolution of any single pollution track. To do the latter, geostationary instruments such as Spinning Enhanced Visible and Infrared Imager (SEVIRI) are needed [III].

## 2.2 Analysing the water path changes in polluted clouds

Large-scale tracks from Norilsk, sampled from years 2000 to 2017, were the main source for studying water path changes in polluted clouds, in order to confirm whether they behave similarly to smaller-scale tracks. Studying pollution tracks enables us to directly compare aerosol-induced perturbations in cloud properties to the properties of nearby unperturbed clouds. In order to utilize this possibility, each large-scale polluted cloud area was sampled from 4 intercardinal directions. For each direction, a line was drawn from unpolluted clouds into polluted clouds, and the pixels in a 60 km wide segment around the gradient-line were classified as polluted or unpolluted using NIR reflectance, following Toll et al., (2019) (Fig. 4).

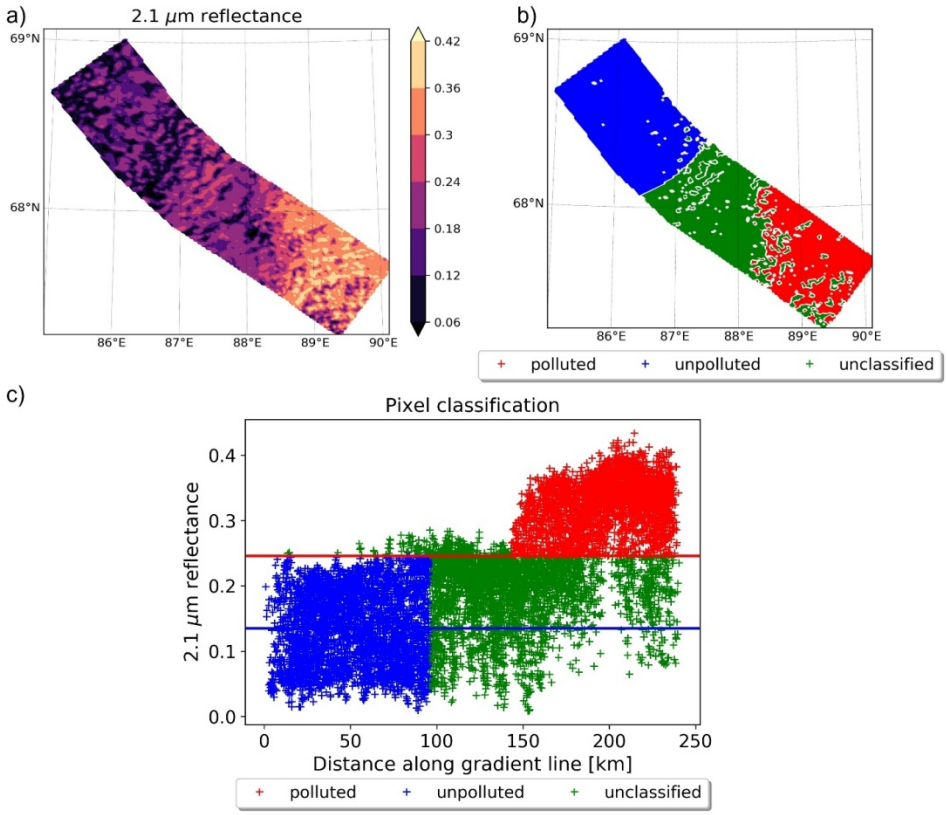


**Figure 4.** Classification of pixels as polluted and unpolluted. (a) A line was manually drawn on the 2.1-μm reflectance image from area with lower reflectance into area with elevated reflectance. A 60-km wide segment around the line was chosen for analysis. (b) Pixels in this segment were classified as polluted (red) or unpolluted (blue). The pixels which were not classified either way are shown here in green and they are not included in the analysis. (c) The blue line is the mean reflectance within the first 20% of the line length from the starting point, where unpolluted clouds are situated. The red line is two standard deviations above the blue line. Pixels are classified as polluted (red) if their reflectance is above the red line and situated in the last 40% of the track, and classified as unpolluted (blue), if their reflectance is under the red line and in the first 40% of the track [I].

After classifying satellite pixels as polluted or unpolluted for each segment, we calculated segment-average cloud properties for polluted and unpolluted clouds [I]. To exclude weak cloud perturbations, we only retained cases where the cloud droplet effective radius was decreased by more than 2 μm in the polluted clouds. This is a relatively strong decrease in cloud droplet size, compared to the average cloud droplet effective radius of 16 μm observed in unperturbed clouds.

## 2.3 Analysing the relationship between track occurrence and environmental conditions

In order to analyse the impact of environmental conditions on the track occurrence, we only studied whether a track exists or not, and the size of the track was not taken into account. We worked out a three-part classification of zero days (no cloud or an ice or mixed-phase cloud), only cloud days (suitable liquid cloud, but no track), and track days (Fig. 5). For each of these three main sites (Norilsk, Thompson and Cherepovets), we classified all days from 2000 to 2019 as zero, only-cloud or track day. It means for Norilsk, some additional tracks were included besides the ones that were analysed for the water path changes.


**Figure 5.** Classification of days. Zero day indicates that track could not have formed, because no suitable cloud is present. Only cloud day means a track could have formed because there is a suitable cloud present, but it didn't form. Track day means that a pollution track has formed in a suitable cloud. These images depict the surroundings of Thompson, Canada, which is marked with a red "x". The pollution track appears in white colour on the rightmost image [II].

Four sources of environmental data were used in subsequent analysis (Table 2). First, we used data from synoptic stations near each location. We chose the times for the meteorological observations to align as closely as possible with the average passing time of the Terra satellite: 06 UTC for Norilsk, 18 UTC for Thompson, and 09 UTC for Cherepovets. Besides in-situ measurements from synoptic stations, we used ERA5 atmospheric reanalysis data (Hersbach et al., 2020) as a second source. The third source was the cloud properties derived from MODIS data. Using the standard 2.1μm retrievals, we averaged six selected properties over an area covering 150 km times 150 km around each location (Platnick et al., 2016). As a fourth source, we calculated the vorticity and atmospheric circulation type around each location for each day, using software cost733class (Philipp et al., 2016). We calculated different classifications, which produced similar results. Therefore, here we present only the Jenkinson Collison types (JCT), which assigns one of 10 classes to each day (Fig. 6). Lastly, we derived other variables from the data we received from the four sources (Table 2).

**Table 2.** Analysed meteorological variables and cloud properties. 'Derived variables' were calculated using the variables from the other columns [II].

| Synoptic stations | ERA5 reanalysis single level variables | ERA5 reanalysis variables on 500 hPa, 700 hPa, 1000 hPa pressure levels | MODIS |
|---|---|---|---|
| Air Temperature<br>Dewpoint temperature<br>Wind speed<br>Wind direction<br>Mean sea level pressure<br>Cloud ceiling<br>Visibility | 2m dewpoint temperature<br>10m u component of wind<br>10m v component of wind<br>2m temperature<br>Boundary layer height<br>Cloud base height<br>Convective available potential energy<br>Convective inhibition<br>Low cloud cover<br>Mean sea level pressure<br>Total precipitation<br>Zero degree level | Temperature<br>Potential vorticity<br>Geopotential<br>U component of wind<br>V component of wind<br>Vertical velocity<br>Vorticity<br>Relative humidity | Cloud droplet effective radius<br>Cloud fraction<br>Cloud optical thickness<br>Cloud top pressure<br>Cloud top temperature<br>Liquid water path |
| Derived variables | | | |
| Cloud droplet number concentration (CDNC, from MODIS data)<br>Lower tropospheric stability (LTS, from reanalysis data)<br>Relative humidity (from station data) | | | |

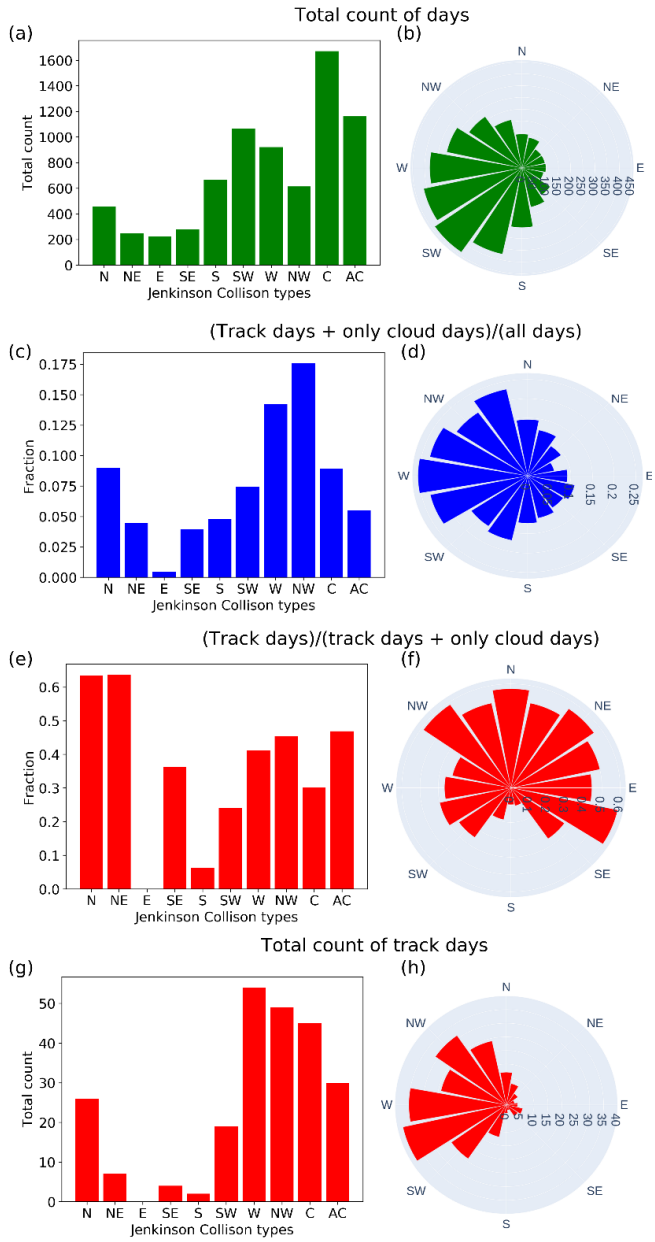


**Figure 6.** The distributions of Jenkinson Collison circulation types in the right column and wind directions at 700 hPa in the left column for Norilsk. (a) and (b) show the total number of days (zero, only-cloud and track days) for each circulation type and wind direction. (c) and (d) show the proportion of liquid-phase cloud days (only-cloud and track days) out of all days in each circulation type/wind direction. (e) and (f) show the fraction of track days out of liquid-phase cloud days. (g) and (h) show the total number of track days for each circulation type and wind direction [II].

# 3. RESULTS

## 3.1 Frequency of track occurrence

We collected 1164 observations from large-scale polluted clouds in the Norilsk area. Here observation means the sample line that was manually drawn from unpolluted clouds into polluted clouds, meaning that the number of actual polluted clouds is about a quarter of all observations. In addition, we collected 99 large-scale observations for various regions for the period 2012 to 2018 (Fig. 3).

We also measured the frequency of occurrence of all tracks for Norilsk, Thompson and Cherepovets, and also of days with liquid-phase clouds, where tracks could potentially form. These frequencies were different for each location. If liquid-phase clouds were present, then tracks formed on 20-37 % of such days [II], depending on the location, but liquid-phase clouds themselves formed on only about 12 % of days (Table 3). On average, we detected 10-13 tracks per year, depending on the location.

**Table 3.** Occurrence frequency of cloud and track days [II].

| | Total number of days in years 2000-2019 | | | Percentages | | |
|---|---|---|---|---|---|---|
| | Zero days (Z) | Only cloud days (C) | Track days (T) | $\frac{C+T}{C+T+Z}$ | $\frac{T}{C+T}$ | $\frac{T}{C+T+Z}$ |
| Norilsk | 6664 | 403 | 237 | 8.7 % | 37 % | 3.2 % |
| Thompson | 6324 | 781 | 199 | 13.5 % | 20.3 % | 2.7 % |
| Cherepovets | 6349 | 700 | 255 | 13 % | 26.7 % | 3.5 % |

## 3.2 Cloud water responses

In the large-scale tracks detected at Norilsk, the radius of cloud droplets dropped on average 50% [I], from 15.9 μm in unpolluted clouds down to 7.9 μm in polluted clouds (Table 4). The frequency distributions of cloud droplet effective radii ($R_{eff}$) for polluted and unpolluted clouds are nearly distinct (Fig. 7). This signals that the observed perturbations were very strong and were caused by aerosol impacts, not by natural variability. Likewise, cloud optical depth (COD), which is proportional to cloud albedo, increased 80% on average (Table 4). The changes in cloud albedo are influenced both by changes in $R_{eff}$ and changes in liquid water path (LWP).

**Table 4.** Average cloud droplet effective radius ($R_{eff}$), liquid water path (LWP) and cloud optical depth (COD) of polluted and unpolluted clouds for large-scale pollution tracks. All cases include observations both from Norilsk and non-Norilsk cases (Fig. 4). Standard deviation is given in the parenthesis [I].

| | Norilsk cases (1164) | | | Non-Norilsk cases (99) | | | All cases (1263) | | |
|---|---|---|---|---|---|---|---|---|---|
| | Unpolluted area | Polluted area | Fractional change | Unpolluted area | Polluted area | Fractional change | Unpolluted area | Polluted area | Fractional change |
| $R_{eff}$ | 15.9 (4) | 7.9 (2) | −0.5 | 14.4 (3) | 8.4 (2) | −0.4 | 15.8 (4) | 7.9 (2) | −0.5 |
| LWP | 142.0 (80) | 125.6 (74) | −0.1 | 184.5 (79) | 141.0 (71) | −0.2 | 145.3 (81) | 126.8 (74) | −0.1 |
| COD | 14.1 (8) | 25.6 (15) | +0.8 | 21.6 (12) | 26.8 (12) | +0.2 | 14.6 (8) | 25.7 (15) | +0.8 |

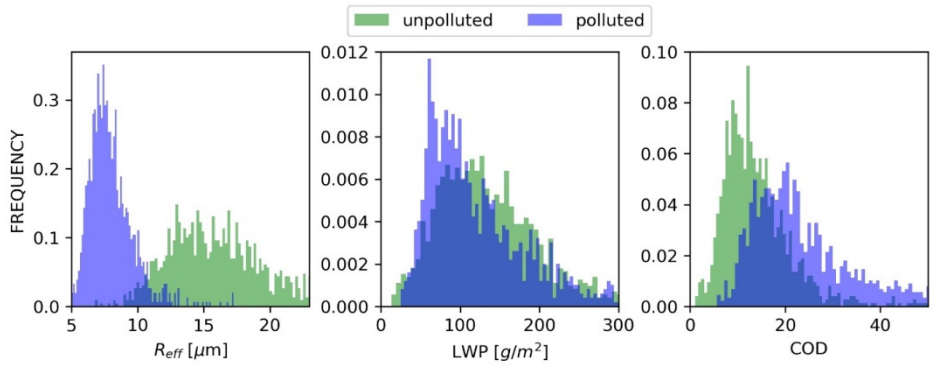


**Figure 7.** Frequency distributions of cloud droplet effective radius ($R_{eff}$), liquid water path (LWP) and cloud optical depth (COD) for polluted and unpolluted clouds in Norilsk [I].

If the changes in the liquid water path were averaged over all analysed tracks, we saw a marginal decrease of cloud water in polluted clouds. However, dramatic changes were observed in individual clouds: LWP could both increase or decrease in the polluted cloud up to 8 times. This is in agreement with Toll et al. (2017) and Toll et al. (2019), where it is explained that whether LWP increases or decreases in an individual cloud is determined by meteorological conditions. For example, in precipitating clouds LWP tends to increase in response to aerosol pollution, and LWP tends to decrease in non-precipitating clouds.

The relative contributions of logarithmic LWP and $R_{eff}$ changes to the relative change in COD are given by

$$\Delta \ln(COD) = \Delta \ln(LWP) - \Delta \ln\left(R_{eff}\right). \qquad (1)$$

The changes in $R_{eff}$ are always negative, meaning that the cloud droplet radius always decreases as a result of aerosol pollution and therefore increases the cloud optical depth, but the changes in LWP are bidirectional, therefore sometimes increasing and sometimes decreasing the optical depth of the cloud. The scale of changes in LWP is much broader than it is in $R_{eff}$. Therefore, the changes in LWP dominate the change in COD in individual clouds. While the average COD was increased in the polluted clouds, in 16% of cases it was also decreased, because the decrease in LWP was so strong that it surpassed the increase of COD that the decrease in $R_{eff}$ brought about.

Both in terms of frequency and magnitude, the LWP increases and decreases compensate and therefore cancel each other out ([I], Fig. 8). Therefore, while the changes in LWP dominate the cloud albedo changes in individual clouds, then on average the changes in $R_{eff}$ are more important, because these changes always only increase the cloud albedo. The frequency distribution of $-\Delta\ln(COD)/\Delta\ln(R_{eff})$ (Equation 1) shows that the relative contribution of LWP

changes to COD changes can be up to four times stronger than the relative contribution of the changes in $R_{eff}$ (Fig. 9). However, the average value of $-\Delta\ln(COD)/\Delta\ln(R_{eff})$ is 0.97, which signifies only a marginal change in LWP and its impact on COD on average.

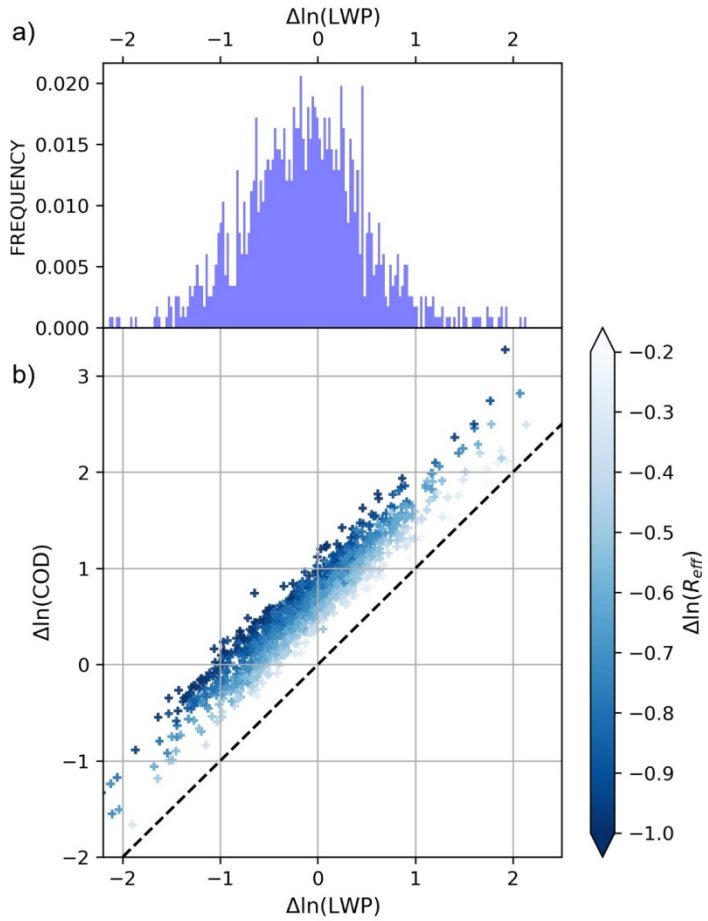


**Figure 8.** (a) Frequency distribution of Δln (LWP). (b) Susceptibility of cloud optical depth (COD) to liquid water path (LWP) changes in Norilsk. The logarithmic changes in cloud droplet effective radii ($R_{eff}$) for individual tracks are given in color. The dashed line is the COD susceptibility to LWP changes if there were no changes in $R_{eff}$ [I].

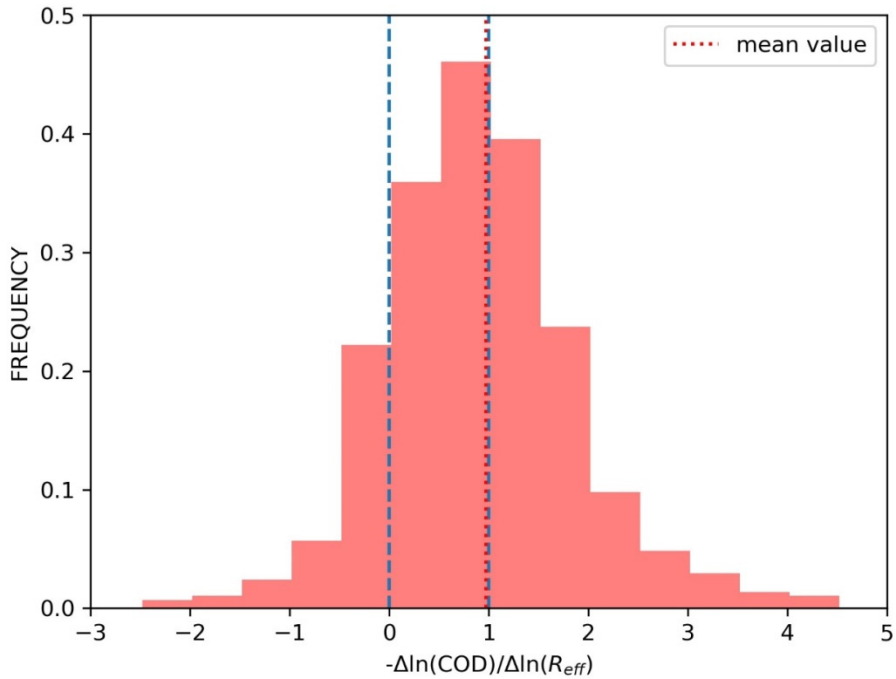


**Figure 9.** Frequency distribution for −Δln (COD)/ Δln ($R_{eff}$) in Norilsk. COD means cloud optical depth and $R_{eff}$ means cloud droplet effective radius. The bin width is 0.5. The mean value is 0.97. Liquid water path is increased in polluted clouds if this ratio is larger than 1 and decreased otherwise. If this ratio is less than than 0, then the COD and the cloud albedo is decreased in the polluted clouds. The values of zero and one are marked with the blue dashed lines.The cloud albedo was decreased in 16.4% of cases. 44% of cases are right of the 1 line [I].

## 3.3 Meteorological dependence of track formation

Norilsk, Thompson and Cherepovets are all located in the middle to higher latitudes of the Northern hemisphere, where western airflow prevails. However, each site has some local variations in the dominant wind directions [II]. Cyclonic circulation dominates in Norilsk, while anti-cyclonic circulation dominates in Cherepovets.

The occurrence of liquid-phase clouds and tracks is strongly dependent on the large-scale atmospheric circulation type in each studied location [II]. This dependence is also largely similar in all three sites. Liquid phase clouds tend to form in cyclonic flows and under wind directions that are shifted clockwise from the wind directions that generally prevail. Therefore, while western airflows prevail in general, liquid-phase clouds form more under NW winds (Fig. 6).

Track days are a subset of liquid-phase cloud days, but have different meteorological dependence from only-cloud days. While liquid-phase clouds themselves tend to form under cyclonic flows, track formation in these clouds is clearly supported more by anti-cyclonic conditions in all three locations (Fig. 6). This finding came out not only from circulation type analysis, but is also supported by the fact that there is stronger large-scale descent and higher mean sea level pressure on track days, compared to only-cloud days (Fig. 10). The wind direction under which tracks tend to form is shifted even more strongly clockwise from the general climatology, compared to the directions which favour only-cloud conditions. The most track-favourable winds are NW to NE in Norilsk, N and E in Thompson and N to E in Cherepovets. Eastern flows are very rare in the analysed locations, but when liquid-phase clouds occur under easterly flow, then tracks are also very likely to occur.

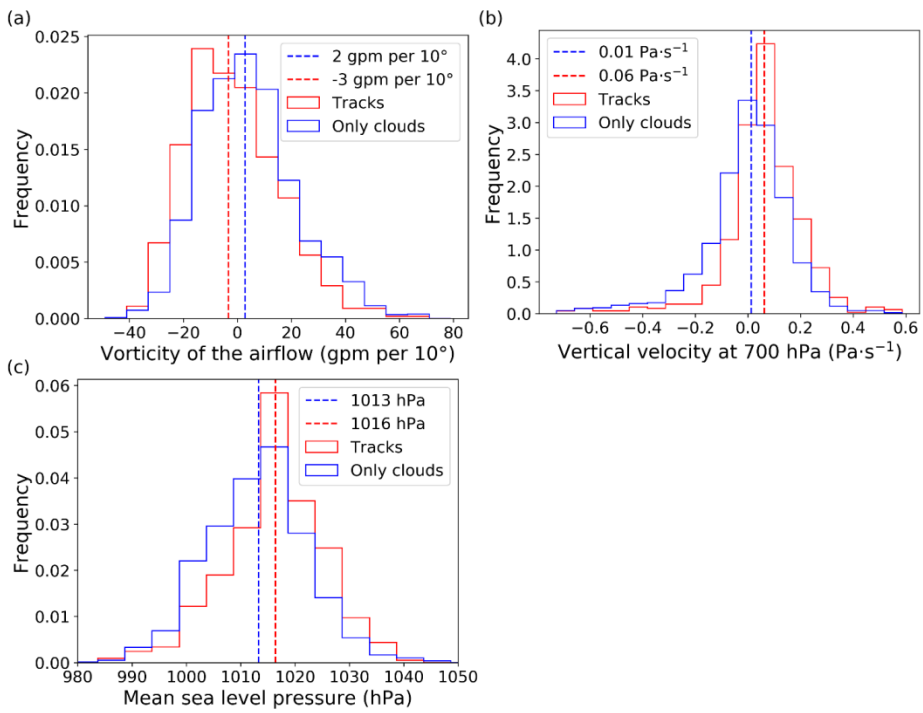


**Figure 10.** (a) Distributions of the vorticity of the airflow for track days (red) and only cloud days (blue). The units of vorticity Z are gpm per 10° at the latitude of the central point of the grid, per 10° latitude. The bin width is 8 gpm. The negative values of Z signify anti-cyclonic airflow and positive values signify cyclonic airflow. (b) Vertical velocity distributions at 700 hPa level for track days (red) and cloud-only days (blue). Negative values of vertical velocity indicate upward motion. The bin width is 0.06 $\mathrm{Pa} \cdot \mathrm{s}^{-1}$. (c) Mean sea level pressure distributions for track days (red) and only cloud days (blue). Station data is used for this figure. Bin width is 5 hPa. The dashed lines show the median values of respective distributions on each image [II].

There are also other relationships between track formation and meteorological conditions besides large-scale circulation [II]. Tracks tend to form in less polluted clouds with larger cloud droplet radii as such clouds are more sensitive to aerosol pollution (Fig. 11). Also thinner clouds, with higher cloud bases, lower cloud tops and smaller liquid water path are more susceptible to aerosol pollution (Fig. 12). Another factor to consider is whether the aerosols can reach the clouds. On days with lower boundary layer height, which limits the vertical height to which pollution disperses, fewer tracks were seen to form (Fig. 13). Generally, tracks are more likely to form under stable conditions. However, not under extremely stable conditions, when vertical transport is more limited.

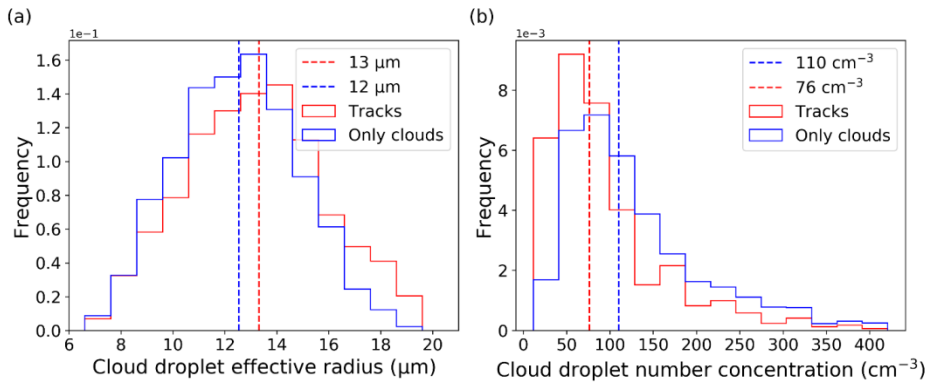


**Figure 11.** (a) Distribution of cloud effective radius for track days (red) and only cloud days (blue). Bin width is 1 μm. (b) Cloud droplet number concentration distributions for track days (red) and cloud-only days (blue). Bin width is 29 cm$^{-3}$. Dashed lines show the median values of respective distributions on each image [II].

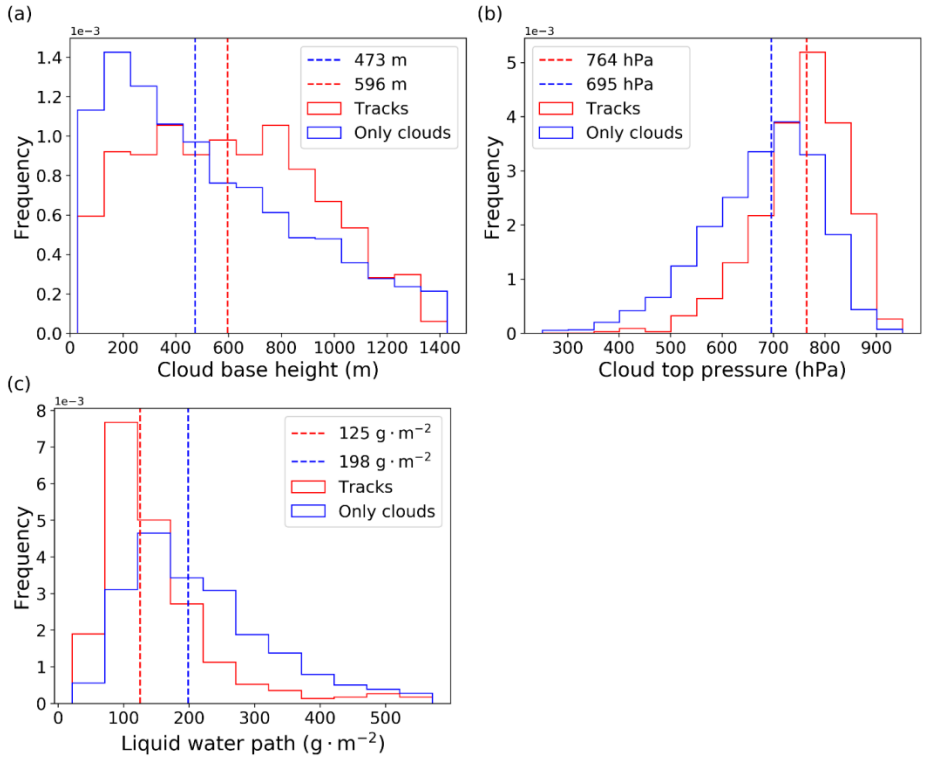


**Figure 12.** Cloud base height (a), cloud top pressure (b) and liquid water path (c) distributions for track days (red) and only cloud days (blue). Reanalysis data are used on (a), and MODIS data are used on (b) and (c). The bin width is 100 m on (a), 50 hPa on (b) and 50 $g \cdot m^{-2}$ on (c). Dashed lines show the median values of respective distributions on each image [II].

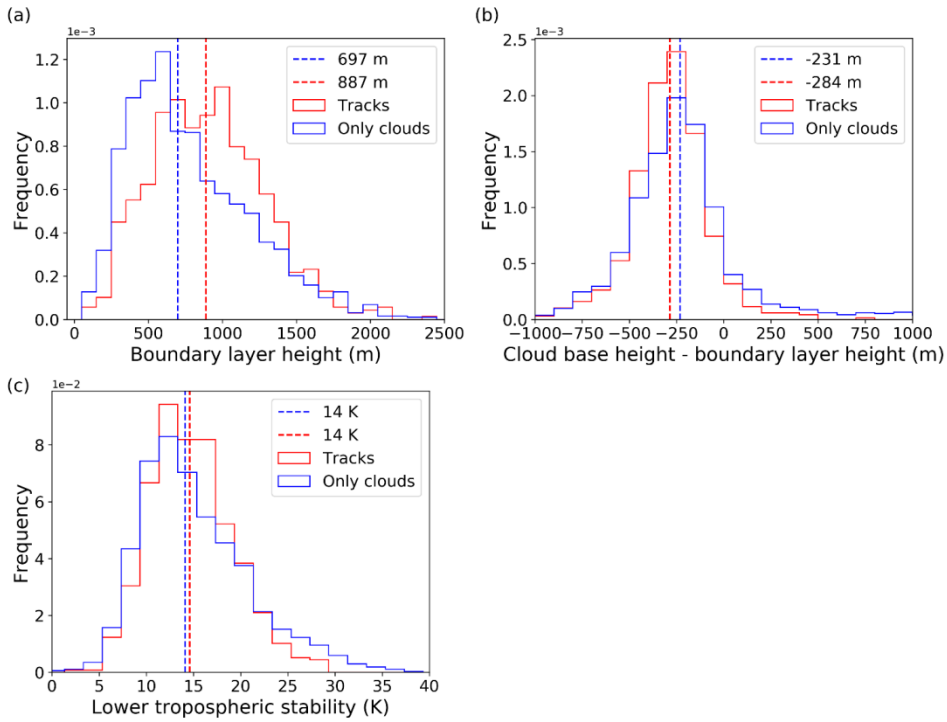


**Figure 13.** (a) Boundary layer height distributions for track days (red) and only cloud days (blue), bin width is 100 m. (b) Distributions of the gap between cloud base and boundary layer for track days (red) and only cloud days (blue), bin width is 100 m. (c) Lower stratospheric stability (LTS) distributions for track (red) and only cloud (blue) days. No tracks form when LTS values are over 29 K. The bin width is 4 K. Dashed lines show the median values of respective distributions on each image [II].

Track days were also characterised by lower relative humidity both at the surface and above clouds, compared to only cloud days (Fig. 14). This trend was most visible at the 700 hPa level. A similar relationship has been observed over oceans (Gryspeerdt et al., 2019). Dry air leads to stronger cloud-top radiative cooling and in-cloud updraughts (Zheng et al., 2016), which increases cloud sensitivity to aerosol perturbation (Twomey, 1959) and could explain the dependence of track formation on relative humidity (Gryspeerdt et al., 2019). Dry air above cloud tops also leads to lower LWP and thinner clouds, where large relative increases in CDNC occur more easily (Chen et al., 2012). However, the occurrence of low relative humidity conditions is correlated to the direction of the large-scale airflow along with other track favouring conditions (Fig. 15), obscuring the exact nature of the causal relationship.

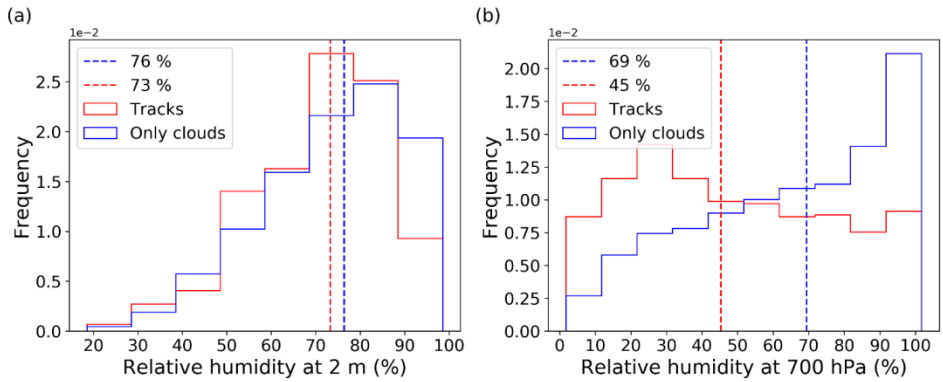


**Figure 14.** Relative humidity distributions for track days (red) and only cloud days (blue). (a) shows station data and (b) reanalysis data at 700 hPa. The bin width is 10 % in both figures. Dashed lines show the median values of respective distributions on each image [II].

Most of the analysed meteorological variables had a similar distribution on track days and on days with NW winds (defined here as the direction between 270 degrees and 360 degrees). In the latter case, we didn't use the classification depicted in Fig. 3, and data from zero-days were included in addition. The distributions were also close to each other on only-cloud days and on days with SW winds (defined here as the direction between 180 degrees and 270 degrees). From the circulation type analysis, we saw that NW flow is more typical for tracks and SW flow for only-cloud days in terms of the absolute number of days. This signifies that wind direction is strongly correlated to the meteorological factors that support track formation, suggesting that the synoptic dependence of track formation can be explained by the cloud type correlated to each meteorological situation.

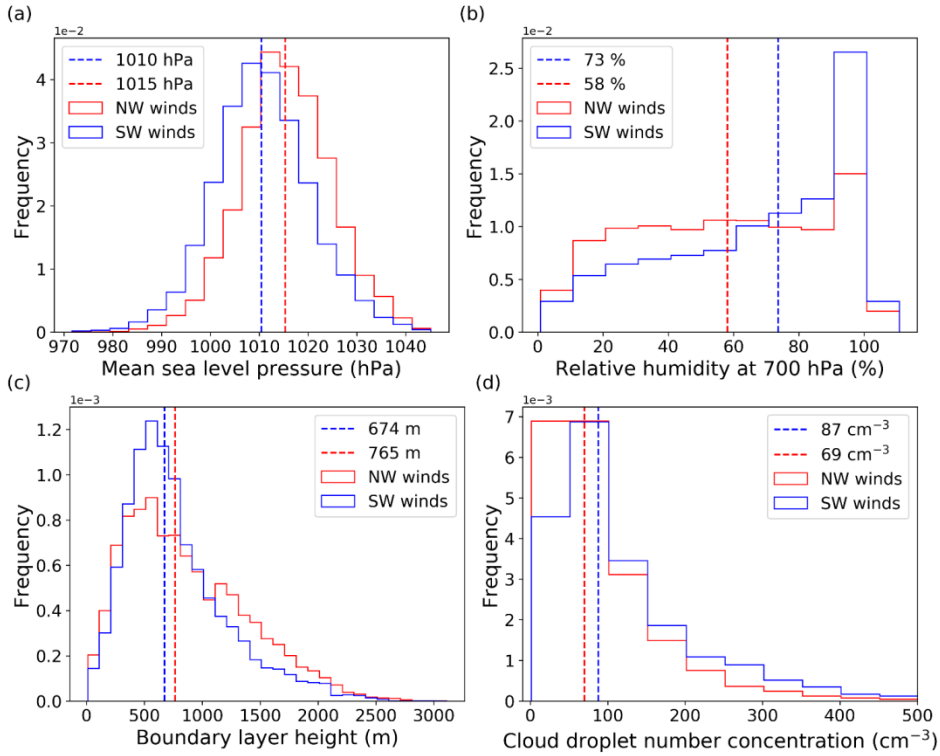


**Figure 15.** (a) Mean sea level pressure (bin width 5 hPa), (b) relative humidity at 700 hPa (bin width 5.5 %), (c) boundary layer height (bin width is 100 m) and (d) cloud droplet number concentration (bin width 50 cm$^{-3}$) distributions for north-west (red) and south-west (blue) winds. Dashed lines show the median values of respective distributions on each image [II].

## 3.4 Diurnal evolution of pollution tracks

The MODIS data that had been previously sampled by Toll et al. (2019) included 8,379 different pollution track segments over Russia, Australia, and Canada. Time-binned MODIS data shows that in the sunlight hours, there is almost always a slight decrease in the cloud water of polluted clouds. However, no diurnal cycle is visible in the LWP response to aerosol (Fig. 16). The datapoints were not distributed evenly over the normalized time coordinate, with the majority of cases being around noontime. Therefore we can't rule out that in the early morning or evening, the cloud water may on average increase or decrease more strongly in the polluted clouds [III].

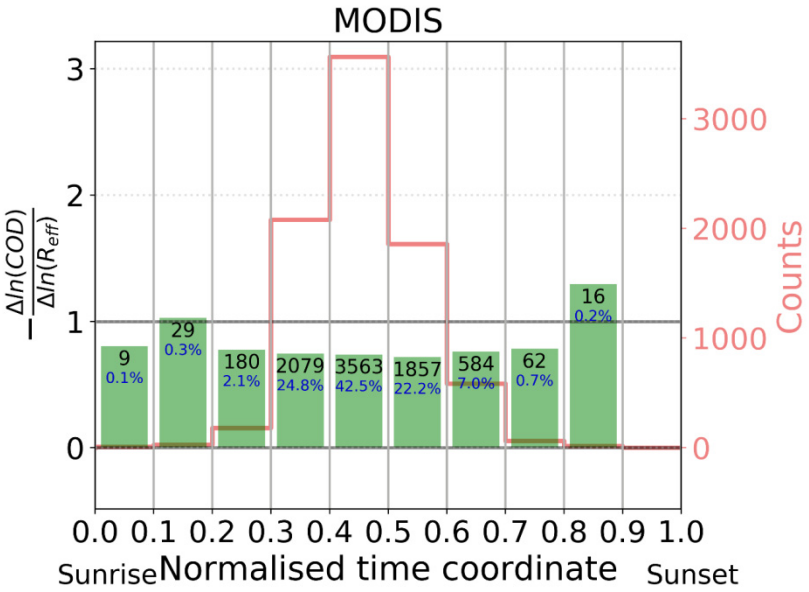


**Figure 16.** The ratio $-\frac{\Delta \ln(\mathrm{COD})}{\Delta \ln(\mathrm{R_{eff}})}$ distributed over normalised time coordinate from sunrise (0.0) to sunset (1.0). The time coordinate value of 0.5 represents the local noon. Total counts of data points are given in black with relative occurrence in blue (at the top of each column) and graphically on the second (right) y-axis. There is no clear diurnal evolution in the liquid water path (LWP) response [III].

# 4. DISCUSSION AND CONCLUSIONS

We analysed strong aerosol-induced cloud perturbations at air pollution hot spots. The droplets in the polluted clouds were on average 50% smaller than in the nearby unpolluted clouds [I]. The analysed polluted clouds cover much larger areas than the polluted cloud tracks analysed in previous studies, which usually extend only to tens of kilometres (Toll et al., 2019). MODIS satellite images show that polluted clouds which extend to hundreds by hundreds of kilometres exist in various places in the world. The track-based studies have been challenged by the difficulty of including narrow ship-track like cloud perturbations in climate models (Mülmenstädt & Feingold, 2018; Possner et al., 2018). However, cloud perturbations on the spatial scale that was used in our study could be modelled directly, because they cover the area of several grid boxes of a typical climate model [I].

Our work doesn't directly address the question of how the radiative effects of tracks compare to weak aerosol perturbations, which cause radiative forcing without forming visible tracks (Possner et al., 2018; Glassmeier et al., 2021). In order to have a strong global effect, the perturbations in cloud properties need to cover a large area. Hence the commonly studied narrow tracks themselves probably do not cause a strong global forcing, and the impact of weak perturbations may be more important. However, our work demonstrates the existence of large-scale strongly-polluted cloud areas, suggesting that strong cloud perturbations may cause a substantial fraction of the global indirect aerosol forcing.

With respect to the changes in cloud water, we determined that these large-scale polluted cloud areas behave similarly to the narrow tracks: there is close compensation between aerosol-induced cloud water increases and decreases ([I], Toll et al., 2019). Our results show that the average decrease in LWP offsets 3% of the radiative forcing through the Twomey effect, meaning that the Twomey effect dominates over the effect of cloud water changes in the radiative forcing on average [I]. This is in agreement with previous analysis on smaller-scale pollution tracks, and invalidates the assumption of universally increased LWP used in climate models.

We have, for the first time, captured the track formation frequency over land [II]. We did it for three locations. Only narrow tracks were observed in Thompson and Cherepovets. In Norilsk, tracks were predominantly large. We determined that on days with liquid clouds, tracks are a rather common phenomenon, forming on 20–37% of such days, depending on the location (Table 3). Norilsk is the only place where we have so far observed the formation of large-scale pollution tracks regularly, although we have analysed individual examples of large-scale pollution tracks in Europe, Asia, North-America and Africa. Detecting large-scale tracks is more difficult than detecting narrow tracks, for the latter can be more easily linked to a single pollution source. It is common in most industrial regions that the distinction between unpolluted and polluted clouds is not as clear as in more pristine locations. It does not indicate, however,

that large-scale tracks, which are more important with respect to global aerosol forcing, are less probable to form than narrow tracks. The formation of large tracks in Norilsk was as frequent as the formation of narrow tracks in Cherepovets and Thompson, and the conditional probability of track formation on days with liquid clouds was even higher (Table 3). However, this may also be due to the much higher pollution level in Norilsk.

In mid-latitudes, the large-scale atmospheric circulation is the most important factor that determines whether tracks form on days with liquid-phase clouds or not. Other supporting factors are pristine or only weakly polluted background cloud decks, thin clouds, stable boundary layer and possibly lower relative humidity, although each of these factors is correlated with certain types of circulation. Anti-cyclonic conditions and northerly, north-westerly and easterly flows are most favourable for track formation in the studied locations.

Specifying the relationship between meteorological conditions and the occurrence of tracks identifies the conditions under which we can expect strong aerosol impacts and also helps to quantify the frequency at which we may expect them (Mülmenstädt and Feingold, 2018). The intermittent occurrence of strong aerosol impact on clouds must be reflected in climate forcing estimates instead of using long-term averaged values, which may lead to biased forcing estimates.

The total number of sampled large-scale cloud perturbations is still relatively limited, but will hopefully be expanded in the future using machine learning methods (Yuan et al., 2019). Our results regarding water content changes in polluted clouds indicate that the cooling effect of aerosols on climate might not be as strong as has been assumed before. However, future work on aerosol-induced changes in cloud coverage and lifetime may still reveal a strong aerosol cooling effect. Despite a weak average change in LWP, a strong increase in cloud fraction is still possible (Rosenfeld et al., 2019). In future work, tracks can be used in the analysis of cloud coverage and lifetime effects in order to further reduce the uncertainty associated with aerosol-cloud interactions.

## FUNDING AND DATA AVAILABILITY

This study was funded by the Estonian Research Council personal research funding grant PSG202. The RGB images (MODIS channels 3-6-7) used for the visual detection of polluted clouds from https://worldview.earthdata.nasa.gov/ were used. The MODIS timestamps and locations of the studied large-scale cloud perturbations are available at http://datadoi.ee/handle/33/190. The dates of the polluted cloud tracks are available at http://datadoi.ee/handle/33/424. The MODIS cloud products MYD06_L2 from Aqua and MOD06_L2 from Terra used in this study are available from the Atmosphere Archive and Distribution System (LAADS) Distributed Active Archive Center (DAAC), https://ladsweb.nascom.nasa.gov/. The data from synoptic stations were downloaded from National Oceanic and Atmospheric Administration's (NOAA) webpage at https://www.ncei.noaa.gov/access/search/data-search/global-hourly. ERA5 hourly data was downloaded from Climate Data Store (CDS), from https://doi.org/10.24381/cds.adbb2d47 for single levels and from https://doi.org/10.24381/cds.bd0915c6 for pressure levels. The MODIS data was downloaded from https://giovanni.gsfc.nasa.gov/giovanni/. The software cost733class for calculating circulation types was worked out during COST action 733 "Harmonisation and Applications of Weather Types Classifications for European Regions".

# SUMMARY IN ESTONIAN

## Tööstusheitmetest tugevalt saastunud pilved aitavad mõista inimtegevuse kliimamõju

Antud väitekirja eesmärk oli uurida, kuidas mõjutavad aerosoolid, õhku pihustunud vedelad ja tahked osakesed, pilvi ja Maa kliimat. Inimtekkelistel aerosoolidel on jahutav kliimamõju, mis tasakaalustab teadmata osa kasvuhoonegaaside soojendavast kliimamõjust. Aga selle jahutava efekti määramatus on ligi kaks korda suurem, kui kasvuhoonegaaside soojendava efekti määramatus, ning see domineerib kogu inimtekkelise kliimamuutuse määramatust. Suurima osa sellest määramatusest moodustab omakorda aerosoolide ja pilvede vastastikmõjuga seotud määramatus. See määramatus kandub üle ka kliimatundlikkuse määramatusesse ja seekaudu tuleviku kliimaprojektsioonide määramatusesse.

Aerosoolid muudavad pilvede omadusi, käitudes kondensatsioonituumadena, mille ümber veeaur saab kondenseeruda pilvepiiskadeks. See viib pilve albeedo kasvuni: mida rohkem kondensatsioonituumasid, seda rohkem pilvepiiskasid. Eeldades, et pilves on fikseeritud hulk vett, peavad need piisad olema väiksemad, kui aerosoolidega mittesaastunud pilvedes, seega saastunud pilvedes on päikesekiirgust tagasipeegeldav pind suurem. Sellel efektil on Maa kliimale jahutav mõju, kuna see suurendab maailmaruumi tagasikiiratava päikesekiirguse hulka. Seda nimetatakse Twomey efektiks, mis on aastakümnete jooksul leidnud eri töödes korduvalt kinnitust. Suur määramatus valitseb aga selle osas, mis juhtub samal ajal pilvede paksuse, eluea ja hulgaga. Kui näiteks pilvede paksus peaks aerosoolisaaste tulemusel drastiliselt vähenema, oleks sellel Maa kliimale soojendav mõju, vaatamata esialgsele albeedo suurenemisele Twomey efekti tõttu. Kui veehulk peaks saaste tulemusel pilvedes aga kasvama, siis võimendaks see veelgi õhusaaste jahutavat mõju.

Isoleeritud saasteallikate puhul on võimalik inimtekkeliste aerosoolidega saastunud pilvi tänu Twomey efektile satelliidipiltide pealt tuvastada. See võimaldab otseselt võrrelda aerosoolidest saastunud pilvede ja nende kõrval asuvate saastumata pilvede omadusi. Sel moel saame me kindlad olla leitud seoste põhjuslikkuses ega pea toetuma pelgalt korrelatiivsetele andmetele.

Selliseid saastunud pilvi nimetatakse ka laevajälgedeks, kuna kõigepealt märgati neid ookeanide kohal, kus pilved on vähem saastunud ja seega aerosoolide suhtes tundlikumad. Laevajäljed on väga kitsad ja nende kogupindala on väike, seetõttu ei mängi nad iseenesest olulist rolli Maa kiirgusbilansis. Antud töös näitame me aga, et mitmel pool maailmas eksisteerivad laevajälgede sarnased saastunud pilved, mis katavad sadade kilomeetrite laiuseid alasid. Nii suured saastunud pilvedega alad võivad mängida olulist rolli Maa kiirgusbilansis. Analüüsisime suuremastaapseid aerosoolidest põhjustatud häiritusi pilvedes Norilski tehase ümber Venemaal ja leidsime, et veehulga muutuste poolest käituvad nad sarnaselt kitsamate saastejälgedega. Kinnitades varasemaid tulemusi, mis saavutati väikeste saastejälgede uurimisel, leidsime, et

individuaalsetes pilvedes võib veehulk nii kasvada kui kahaneda. Kõiki juhtumeid keskmistades selgus, et need erisuunalised efektid kompenseerivad üksteist, ning veehulga keskmine muutus osutus marginaalseks. See lükkab ümber kliimamudelites kasutatud eelduse, mille kohaselt veehulk pilvedes saaste tulemusena üksnes kasvab.

Samuti uurisime jälgede esinemise sagedust ja nende sõltuvust meteoroloogilistest tingimustest. Analüüsides saastejälgede tekkimist Norilskis ja Cherepovetsis Venemaal ning Thompsonis Kanadas, leidsime, et saastejäljed tekivad sõltuvalt asukohast 20–37% vedela faasiga pilvedega päevadest. Suuremastaapne tsirkulatsioon on olulisim tegur, mis määrab, kas saastejälg antud päeval tekib või ei teki. Saastejäljed tekivad rohkem antitsüklonaalsetes tingimustes ning loode-, põhja-, kirde- ja idavoolude korral. Saastejälgede tekkimiseks sobivate tingimuste väljaselgitamine on tähtis, et määrata täpsemini, kui sagedasti võime eeldada aerosoolide tugevat mõju pilvede omadustele ja sellest lähtuvat kliimamõju. Arvutades aerosoolide kiirguslikku mõju, peame arvestama saastunud pilvede esinemise katkendlikku loomust, mitte kasutama ajas keskmistatud väärtuseid.

Analüüsitud saastunud pilvede hulk oli suhteliselt väike, aga tulevikus saab seda kasvatada masinõppe meetodite abil. Meie tulemused pilve veehulga muutuste kohta viitavad sellele, et aerosoolidel ei ole nii tugevat jahutavat mõju pilvede veesisalduse kasvu tõttu  nagu on varem eeldatud. Aga ei saa välistada, et aerosoolidel on tugev jahutav mõju pilvede eluea või katvuse muutuste tõttu. Tulevikus on võimalik saastunud pilvi kasutada ka nende efektide uurimiseks ja seeläbi vähendada aerosoolide kliimamõju määramatust veelgi.

# REFERENCES


Albrecht, B. A.: Aerosols, cloud microphysics, and fractional cloudiness, Science, 245(4923), 1227–1230, 1989.

Andreae, M., Jones, C. and Cox, P.: Strong present-day aerosol cooling implies a hot future. Nature 435, 1187–1190, 2005.

Bellouin, N., Boucher, O., Haywood, J., and Reddy, M. S.: Global estimate of aerosol direct radiative forcing from satellite measurements, Nature, 438(7071), 1138–1141, 2005

Bellouin, N., Quaas, J., Gryspeerdt, E., Kinne, S., Stier, P., Watson-Parris, D., Boucher, O., Carslaw, K.S., Christensen, M., Daniau, A.L. and Dufresne, J.L.: Bounding global aerosol radiative forcing of climate change, Reviews of Geophysics, 58(1), p.e2019RG000660, 2020.

Carn, S. A., Krueger, A. J., Krotkov, N. A. and Gray, M. A.: Fire at Iraqi sulfur plant emits SO2 clouds detected by Earth Probe TOMS, Geophysical research letters, 31(19), 2004.

Chen, Y. C., Christensen, M. W., Xue, L., Sorooshian, A., Stephens, G. L., Rasmussen, R. M., Seinfeld, J. H.: Occurrence of lower cloud albedo in ship tracks, Atmospheric Chemistry and Physics, 12(17), 8223–8235, 2012.

Coakley Jr, J. A., Bernstein, R. L. and Durkee, P. A.: Effect of ship-stack effluents on cloud reflectivity, Science, 237(4818), 1020–1022, 1987.

Forster, P., Storelvmo T., Armour K., Collins W., Dufresne J. L., Frame D., Lunt D. J., Mauritsen T., Palmer M. D., Watanabe M., Wild M., Zhang H.: The Earth's Energy Budget, Climate Feedbacks, and Climate Sensitivity, Climate Change 2021: The Physical Science Basis, Contribution of Working Group I 40 to the Sixth Assessment Report of the Intergovernmental Panel on Climate Change, Cambridge University Press, 2021.

Glassmeier, F., Hoffmann, F., Johnson, J. S., Yamaguchi, T., Carslaw, K. S., Feingold, G.: Aerosol-cloud-climate cooling overestimated by ship-track data, Science, 371(6528), 485–489, 2021.

Gryspeerdt, E., Smith, T. W., O'Keeffe, E., Christensen, M. W., and Goldsworth, F. W.: The impact of ship emission controls recorded by cloud properties, Geophysical Research Letters, 46(21), 12547–12555, 2019.

Hersbach, H., Bell, B., Berrisford, P., Hirahara, S., Horányi, A., Muñoz-Sabater, J., Nicolas, J., Peubey, C., Radu, R., Schepers, D. and Simmons, A.: The ERA5 global reanalysis, Q J R Meteorol Soc., 146: 1999– 2049, 2020.

Myhre, G., Samset, B.H., Schulz, M., Balkanski, Y., Bauer, S., Berntsen, T.K., Bian, H., Bellouin, N., Chin, M., Diehl, T. and Easter, R.C.: Radiative forcing of the direct aerosol effect from AeroCom Phase II simulations, Atmospheric Chemistry and Physics, 13(4), pp.1853–1877, 2013.

Mülmenstädt, J., Feingold, G.: The Radiative Forcing of Aerosol–Cloud Interactions in Liquid Clouds: Wrestling and Embracing Uncertainty, Curr Clim Change Rep 4, 23–40, 2018.

Philipp, A., Beck, C., Huth, R. and Jacobeit, J.: Development and comparison of circulation type classifications using the COST 733 dataset and software, Int. J. Climatol., 36: 2673–2691, 2016.

Platnick, S., Meyer, K.G., King, M.D., Wind, G., Amarasinghe, N., Marchant, B., Arnold, G.T., Zhang, Z., Hubanks, P.A., Holz, R.E. and Yang, P.: The MODIS cloud optical and microphysical products: Collection 6 updates and examples from

Terra and Aqua, IEEE Transactions on Geoscience and Remote Sensing, 55(1), pp.502–525, 2016.
Possner, A., Wang, H., Wood, R., Caldeira, K., Ackerman, T.: The efficacy of aerosol-cloud-radiative perturbations from near-surface emissions in deep open-cell stratocumuli, Atmospheric Chemistry and Physics, 18, 17475–17488, 2018.
Rosenfeld, D., Zhu, Y., Wang, M., Zheng, Y., Goren, T. and Yu, S.: Aerosol-driven droplet concentrations dominate coverage and water of oceanic low-level clouds, Science, 363(6427), 2019.
Smith, S. J., Aardenne, J. V., Klimont, Z., Andres, R. J., Volke, A. and Delgado Arias, S.: Anthropogenic sulfur dioxide emissions: 1850–2005, Atmospheric Chemistry and Physics, 11(3), 1101–1116, 2011.
Stevens, B., Sherwood, S. C., Bony, S. and Webb, M. J.: Prospects for narrowing bounds on Earth's equilibrium climate sensitivity, Earth's Future, 4(11), 512–522, 2016.
Toll, V., Christensen, M., Gassó, S. and Bellouin, N.: Volcano and Ship Tracks Indicate Excessive Aerosol-Induced Cloud Water Increases in a Climate Model, Geophysical research letters, 44(24), 12–492, 2017.
Toll, V., Christensen, M., Quaas, J., and Bellouin, N.: Weak average liquid-cloud-water response to anthropogenic aerosols, Nature, 572(7767), 51–55, 2019.
Twomey, S.: The nuclei of natural cloud formation part II: The supersaturation in natural clouds and the variation of cloud dropletconcentration, Geofisica Pura e Applicata,43(1), 243–249, 1959.
Twomey, S.: Pollution and the planetary albedo. Atmospheric Environment (1967), 8(12), 1251–1256, 1974.
Yuan, T., Wang, C., Song, H., Platnick, S., Meyer, K., Oreopoulos, L.: Automatically Finding Ship Tracks to Enable Large-Scale Analysis of Aerosol-Cloud Interactions, Geophysical Research Letters, 2019.
Zheng, Y., Rosenfeld, D. and Li, Z.: Quantifying cloud base updraft speeds of marine stratocumulus from cloud top radiative cooling, Geophysical Research Letters,43, 11,407–11,413, 2016.

# ACKNOWLEDGEMENTS

Foremost I wish to thank my supervisors, Dr Velle Toll and Dr Piia Post, for supporting me throughout my PhD studies. I am very grateful for their advice and the time and effort they put into scientific discussions and reviewing my work. I appreciate their patience with me and their keen interest in my progress.

I also wish to thank everyone else in the Atmospheric Physics Lab for providing the place and context where my thesis could be written. My special thanks belong to Jorma Rahu, who was always willing to help me with any kind of question. And I could not forget Prof. Rein Rõõm, supervisor of my Bachelor's and Master's thesis, without whom I would never have made it to the PhD. I'm also very thankful to the University of Tartu and the Institute of Physics for the ten significant years, or one third of my life, that I have spent there.

I thank coauthors Prof. Nicolas Bellouin and Dr Edward Gryspeerdt for their valuable contributions, which helped to improve my research papers.

I am very grateful to the entire KappaZeta team for allowing me a part-time job and enough time to work on my thesis. Your patience is highly appreciated.

I wish to thank my high school teacher Helen Kaasik, who gave me the confidence that I could be good at maths.

I thank my flatmates Joonas Järve and Mathias Are, for making my life brighter in stressful times. And I thank my family for all the support and encouragement.

# PUBLICATIONS

# CURRICULUM VITAE

**Name:** Heido Trofimov
**Date of birth:** February 22, 1993
**Citizenship:** Estonian
**Gender:** Male
**E-mail:** heido.trofimov@ut.ee

**Education**

| | |
|---|---|
| 2018–2022 | University of Tartu; PhD in Physics |
| 2016–2018 | University of Tartu; MSc in Physics |
| 2012–2016 | University of Tartu; BSc in Physics |

**Languages**

Estonian (native), English (fluent)

**Professional employment**

| | |
|---|---|
| 2020–... | KappaZeta Ltd; software developer |
| 2020–... | University of Tartu, Institute of Physics; specialist |
| 2016–2018 | The Estonian Environment Agency, Forecast Models Department; chief specialist |

**Research interests**

Natural sciences and engineering, atmosphere physics, climatology, remote sensing, radiative transfer in the atmosphere, aerosol-cloud interaction

**Publications**

Rahu, Jorma; **Trofimov, Heido**; Post, Piia; Toll, Velle (2022). Diurnal Evolution of Cloud Water Responses to Aerosols. Journal of Geophysical Research Atmospheres, 127 (10)

**Trofimov, Heido**; Post, Piia; Gryspeerdt, Edward; Toll, Velle (2022). Meteorological Conditions Favorable for Strong Anthropogenic Aerosol Impacts on Clouds. Journal of Geophysical Research Atmospheres, 127 (4)

Domnich, Marharyta; Sünter, Indrek; **Trofimov, Heido**; Wold, Olga; Harun, Fariha; Kostiukhin, Anton; Järveoja, Mihkel; Veske, Mihkel; Tamm, Tanel; Voormansik, Kaupo; Olesk, Aire (2021). KappaMask: AI-Based Cloudmask Processor for Sentinel-2. Remote Sensing, 13(20), 4100.

Toll, Velle; **Trofimov, Heido**; Rahu, Jorma; Post, Piia (2021). Polluted cloud lines in satellite snapshots and satellite climatologies. Polluted cloud lines in satellite snapshots and satellite climatologies. EGU GA abstracts.

Toll, Velle; **Trofimov, Heido**; Rahu, Jorma (2021). Natural Experiments for Studying Anthropogenic Aerosol Impacts on Clouds. AMS abstracts.

**Trofimov, Heido**; Toll, Velle (2021). Meteorological conditions favourable for strong aerosol impacts on clouds. Meteorological conditions favourable for

strong aerosol impacts on clouds: Virtual EGU General Assembly, 19–30 April, 2021. European Geoscience Union. vPICO oresentation.

**Trofimov, Heido**; Bellouin, Nicolas; Toll, Velle (2020). Large-Scale Industrial Cloud Perturbations Confirm Bidirectional Cloud Water Responses to Anthropogenic Aerosols. Journal of Geophysical Research Atmospheres, 125 (14), ARTN e2020JD032575.

**Trofimov, Heido**; Toll, Velle (2020). Large-scale industrial cloud perturbations confirm bidirectional cloud water responses to anthropogenic aerosols. In: EGU General Assembly 2020. EGU General Assembly 2020. Virtual poster presentation.

Toll, Velle; Bellouin, Nicolas; Christensen, Matthew; Quaas, Johannes; **Trofimov, Heido**; Rahu, Jorma; Diamond, Michael (2020). Polluted cloud tracks across spatial and temporal scales. AGU abstracts.

# ELULOOKIRJELDUS

**Nimi:** Heido Trofimov
**Sünniaeg:** 22. veebruar 1993
**Kodakondsus:** Eestlane
**Sugu:** Mees
**E-mail:** heido.trofimov@ut.ee

**Haridus**

| | |
|---|---|
| 2018–2022 | Tartu Ülikool, füüsika õppekava, PhD |
| 2016–2018 | Tartu Ülikool, füüsika õppekava, MSc |
| 2012–2016 | Tartu Ülikool, füüsika õppekava, BSc |

**Keelteoskus**

Eesti (emakeel), inglise (sorav)

**Töökogemus**

| | |
|---|---|
| 2020–... | KappaZeta AS, tarkvaraarendaja |
| 2020–... | Tartu Ülikool, Füüsika instituut, spetsialist |
| 2016–2018 | Keskkonnaagentuur, prognoosmudelite osakond, peaspetsialist |

**Teadustöö põhisuunad**

Loodusteadused ja tehnika, atmosfäärifüüsika, klimatoloogia, kaugseire, atmosfääri kiirguslevi, aerosoolide ja pilvede vastastikmõju

**Publikatsioonid**

Rahu, Jorma; **Trofimov, Heido**; Post, Piia; Toll, Velle (2022). Diurnal Evolution of Cloud Water Responses to Aerosols. Journal of Geophysical Research Atmospheres, 127 (10)

**Trofimov, Heido**; Post, Piia; Gryspeerdt, Edward; Toll, Velle (2022). Meteorological Conditions Favorable for Strong Anthropogenic Aerosol Impacts on Clouds. Journal of Geophysical Research Atmospheres, 127 (4)

Domnich, Marharyta; Sünter, Indrek; **Trofimov, Heido**; Wold, Olga; Harun, Fariha; Kostiukhin, Anton; Järveoja, Mihkel; Veske, Mihkel; Tamm, Tanel; Voormansik, Kaupo; Olesk, Aire (2021). KappaMask: AI-Based Cloudmask Processor for Sentinel-2. Remote Sensing, 13(20), 4100.

Toll, Velle; **Trofimov, Heido**; Rahu, Jorma; Post, Piia (2021). Polluted cloud lines in satellite snapshots and satellite climatologies. Polluted cloud lines in satellite snapshots and satellite climatologies. EGU GA abstracts.

Toll, Velle; **Trofimov, Heido**; Rahu, Jorma (2021). Natural Experiments for Studying Anthropogenic Aerosol Impacts on Clouds. AMS abstracts.

**Trofimov, Heido**; Toll, Velle (2021). Meteorological conditions favourable for strong aerosol impacts on clouds. Meteorological conditions favourable for

strong aerosol impacts on clouds: Virtual EGU General Assembly, 19–30 April, 2021. European Geoscience Union. vPICO oresentation.

**Trofimov, Heido**; Bellouin, Nicolas; Toll, Velle (2020). Large-Scale Industrial Cloud Perturbations Confirm Bidirectional Cloud Water Responses to Anthropogenic Aerosols. Journal of Geophysical Research Atmospheres, 125 (14), ARTN e2020JD032575.

**Trofimov, Heido**; Toll, Velle (2020). Large-scale industrial cloud perturbations confirm bidirectional cloud water responses to anthropogenic aerosols. In: EGU General Assembly 2020. EGU General Assembly 2020. Virtual poster presentation.

Toll, Velle; Bellouin, Nicolas; Christensen, Matthew; Quaas, Johannes; **Trofimov, Heido**; Rahu, Jorma; Diamond, Michael (2020). Polluted cloud tracks across spatial and temporal scales. AGU abstracts.

# DISSERTATIONES PHYSICAE UNIVERSITATIS TARTUENSIS

1. **Andrus Ausmees.** XUV-induced electron emission and electron-phonon interaction in alkali halides. Tartu, 1991.
2. **Heiki Sõnajalg.** Shaping and recalling of light pulses by optical elements based on spectral hole burning. Tartu, 1991.
3. **Sergei Savihhin.** Ultrafast dynamics of F-centers and bound excitons from picosecond spectroscopy data. Tartu, 1991.
4. **Ergo Nõmmiste.** Leelishalogeniidide röntgenelektronemissioon kiiritamisel footonitega energiaga 70–140 eV. Tartu, 1991.
5. **Margus Rätsep.** Spectral gratings and their relaxation in some low-temperature impurity-doped glasses and crystals. Tartu, 1991.
6. **Tõnu Pullerits.** Primary energy transfer in photosynthesis. Model calculations. Tartu, 1991.
7. **Olev Saks.** Attoampri diapasoonis voolude mõõtmise füüsikalised alused. Tartu, 1991.
8. **Andres Virro.** AlGaAsSb/GaSb heterostructure injection lasers. Tartu, 1991.
9. **Hans Korge.** Investigation of negative point discharge in pure nitrogen at atmospheric pressure. Tartu, 1992.
10. **Jüri Maksimov.** Nonlinear generation of laser VUV radiation for high-resolution spectroscopy. Tartu, 1992.
11. **Mark Aizengendler.** Photostimulated transformation of aggregate defects and spectral hole burning in a neutron-irradiated sapphire. Tartu, 1992.
12. **Hele Siimon.** Atomic layer molecular beam epitaxy of $A^2B^6$ compounds described on the basis of kinetic equations model. Tartu, 1992.
13. **Tõnu Reinot.** The kinetics of polariton luminescence, energy transfer and relaxation in anthracene. Tartu, 1992.
14. **Toomas Rõõm.** Paramagnetic $H^{2-}$ and $F^+$ centers in CaO crystals: spectra, relaxation and recombination luminescence. Tallinn, 1993.
15. **Erko Jalviste.** Laser spectroscopy of some jet-cooled organic molecules. Tartu, 1993.
16. **Alvo Aabloo.** Studies of crystalline celluloses using potential energy calculations. Tartu, 1994.
17. **Peeter Paris.** Initiation of corona pulses. Tartu, 1994.
18. **Павел Рубин.** Локальные дефектные состояния в $CuO_2$ плоскостях высокотемпературных сверхпроводников. Тарту, 1994.
19. **Olavi Ollikainen.** Applications of persistent spectral hole burning in ultrafast optical neural networks, time-resolved spectroscopy and holographic interferometry. Tartu, 1996.
20. **Ülo Mets.** Methodological aspects of fluorescence correlation spectroscopy. Tartu, 1996.
21. **Mikhail Danilkin.** Interaction of intrinsic and impurity defects in CaS:Eu luminophors. Tartu, 1997.

22. **Ирина Кудрявцева.** Создание и стабилизация дефектов в кристаллах KBr, KCl, RbCl при облучении ВУФ-радиацией. Тарту, 1997.
23. **Andres Osvet.** Photochromic properties of radiation-induced defects in diamond. Tartu, 1998.
24. **Jüri Örd.** Classical and quantum aspects of geodesic multiplication. Tartu, 1998.
25. **Priit Sarv.** High resolution solid-state NMR studies of zeolites. Tartu, 1998.
26. **Сергей Долгов.** Электронные возбуждения и дефектообразование в некоторых оксидах металлов. Тарту, 1998.
27. **Kaupo Kukli.** Atomic layer deposition of artificially structured dielectric materials. Tartu, 1999.
28. **Ivo Heinmaa.** Nuclear resonance studies of local structure in $RBa_2Cu_3O_{6+x}$ compounds. Tartu, 1999.
29. **Aleksander Shelkan.** Hole states in $CuO_2$ planes of high temperature superconducting materials. Tartu, 1999.
30. **Dmitri Nevedrov.** Nonlinear effects in quantum lattices. Tartu, 1999.
31. **Rein Ruus.** Collapse of 3d (4f) orbitals in 2p (3d) excited configurations and its effect on the x-ray and electron spectra. Tartu, 1999.
32. **Valter Zazubovich.** Local relaxation in incommensurate and glassy solids studied by Spectral Hole Burning. Tartu, 1999.
33. **Indrek Reimand.** Picosecond dynamics of optical excitations in GaAs and other excitonic systems. Tartu, 2000.
34. **Vladimir Babin.** Spectroscopy of exciton states in some halide macro- and nanocrystals. Tartu, 2001.
35. **Toomas Plank.** Positive corona at combined DC and AC voltage. Tartu, 2001.
36. **Kristjan Leiger.** Pressure-induced effects in inhomogeneous spectra of doped solids. Tartu, 2002.
37. **Helle Kaasik.** Nonperturbative theory of multiphonon vibrational relaxation and nonradiative transitions. Tartu, 2002.
38. **Tõnu Laas.** Propagation of waves in curved spacetimes. Tartu, 2002.
39. **Rünno Lõhmus.** Application of novel hybrid methods in SPM studies of nanostructural materials. Tartu, 2002.
40. **Kaido Reivelt.** Optical implementation of propagation-invariant pulsed free-space wave fields. Tartu, 2003.
41. **Heiki Kasemägi.** The effect of nanoparticle additives on lithium-ion mobility in a polymer electrolyte. Tartu, 2003.
42. **Villu Repän.** Low current mode of negative corona. Tartu, 2004.
43. **Алексей Котлов.** Оксианионные диэлектрические кристаллы: зонная структура и электронные возбуждения. Tartu, 2004.
44. **Jaak Talts.** Continuous non-invasive blood pressure measurement: comparative and methodological studies of the differential servo-oscillometric method. Tartu, 2004.
45. **Margus Saal.** Studies of pre-big bang and braneworld cosmology. Tartu, 2004.

46. **Eduard Gerškevitš.** Dose to bone marrow and leukaemia risk in external beam radiotherapy of prostate cancer. Tartu, 2005.
47. **Sergey Shchemelyov.** Sum-frequency generation and multiphoton ionization in xenon under excitation by conical laser beams. Tartu, 2006.
48. **Valter Kiisk.** Optical investigation of metal-oxide thin films. Tartu, 2006.
49. **Jaan Aarik.** Atomic layer deposition of titanium, zirconium and hafnium dioxides: growth mechanisms and properties of thin films. Tartu, 2007.
50. **Astrid Rekker.** Colored-noise-controlled anomalous transport and phase transitions in complex systems. Tartu, 2007.
51. **Andres Punning.** Electromechanical characterization of ionic polymer-metal composite sensing actuators. Tartu, 2007.
52. **Indrek Jõgi.** Conduction mechanisms in thin atomic layer deposited films containing $TiO_2$. Tartu, 2007.
53. **Aleksei Krasnikov.** Luminescence and defects creation processes in lead tungstate crystals. Tartu, 2007.
54. **Küllike Rägo.** Superconducting properties of $MgB_2$ in a scenario with intra- and interband pairing channels. Tartu, 2008.
55. **Els Heinsalu.** Normal and anomalously slow diffusion under external fields. Tartu, 2008.
56. **Kuno Kooser.** Soft x-ray induced radiative and nonradiative core-hole decay processes in thin films and solids. Tartu, 2008.
57. **Vadim Boltrushko.** Theory of vibronic transitions with strong nonlinear vibronic interaction in solids. Tartu, 2008.
58. **Andi Hektor.** Neutrino Physics beyond the Standard Model. Tartu, 2008.
59. **Raavo Josepson.** Photoinduced field-assisted electron emission into gases. Tartu, 2008.
60. **Martti Pärs.** Study of spontaneous and photoinduced processes in molecular solids using high-resolution optical spectroscopy. Tartu, 2008.
61. **Kristjan Kannike.** Implications of neutrino masses. Tartu, 2008.
62. **Vigen Issahhanjan.** Hole and interstitial centres in radiation-resistant MgO single crystals. Tartu, 2008.
63. **Veera Krasnenko.** Computational modeling of fluorescent proteins. Tartu, 2008.
64. **Mait Müntel.** Detection of doubly charged higgs boson in the CMS detector. Tartu, 2008.
65. **Kalle Kepler.** Optimisation of patient doses and image quality in diagnostic radiology. Tartu, 2009.
66. **Jüri Raud.** Study of negative glow and positive column regions of capillary HF discharge. Tartu, 2009.
67. **Sven Lange.** Spectroscopic and phase-stabilisation properties of pure and rare-earth ions activated $ZrO_2$ and $HfO_2$. Tartu, 2010.
68. **Aarne Kasikov.** Optical characterization of inhomogeneous thin films. Tartu, 2010.
69. **Heli Valtna-Lukner.** Superluminally propagating localized optical pulses. Tartu, 2010.

70. **Artjom Vargunin.** Stochastic and deterministic features of ordering in the systems with a phase transition. Tartu, 2010.
71. **Hannes Liivat.** Probing new physics in e+e− annihilations into heavy particles via spin orientation effects. Tartu, 2010.
72. **Tanel Mullari.** On the second order relativistic deviation equation and its applications. Tartu, 2010.
73. **Aleksandr Lissovski.** Pulsed high-pressure discharge in argon: spectroscopic diagnostics, modeling and development. Tartu, 2010.
74. **Aile Tamm.** Atomic layer deposition of high-permittivity insulators from cyclopentadienyl-based precursors. Tartu, 2010.
75. **Janek Uin.** Electrical separation for generating standard aerosols in a wide particle size range. Tartu, 2011.
76. **Svetlana Ganina.** Hajusandmetega ülesanded kui üks võimalus füüsikaõppe efektiivsuse tõstmiseks. Tartu, 2011
77. **Joel Kuusk.** Measurement of top-of-canopy spectral reflectance of forests for developing vegetation radiative transfer models. Tartu, 2011.
78. **Raul Rammula**. Atomic layer deposition of $HfO_2$ – nucleation, growth and structure development of thin films. Tartu, 2011.
79. **Сергей Наконечный.** Исследование электронно-дырочных и интерстициал-вакансионных процессов в монокристаллах MgO и LiF методами термоактивационной спектроскопии. Тарту, 2011.
80. **Niina Voropajeva.** Elementary excitations near the boundary of a strongly correlated crystal. Tartu, 2011.
81. **Martin Timusk.** Development and characterization of hybrid electro-optical materials. Tartu, 2012, 106 p.
82. **Merle Lust.** Assessment of dose components to Estonian population. Tartu, 2012, 84 p.
83. **Karl Kruusamäe.** Deformation-dependent electrode impedance of ionic electromechanically active polymers. Tartu, 2012, 128 p.
84. **Liis Rebane.** Measurement of the $W \to \tau\nu$ cross section and a search for a doubly charged Higgs boson decaying to τ-leptons with the CMS detector. Tartu, 2012, 156 p.
85. **Jevgeni Šablonin.** Processes of structural defect creation in pure and doped MgO and NaCl single crystals under condition of low or super high density of electronic excitations. Tartu, 2013, 145 p.
86. **Riho Vendt**. Combined method for establishment and dissemination of the international temperature scale. Tartu, 2013, 108 p.
87. **Peeter Piksarv.** Spatiotemporal characterization of diffractive and non-diffractive light pulses. Tartu, 2013, 156 p.
88. **Anna Šugai.** Creation of structural defects under superhigh-dense irradiation of wide-gap metal oxides. Tartu, 2013, 108 p.
89. **Ivar Kuusik.** Soft X-ray spectroscopy of insulators. Tartu, 2013, 113 p.
90. **Viktor Vabson**. Measurement uncertainty in Estonian Standard Laboratory for Mass. Tartu, 2013, 134 p.

91. **Kaupo Voormansik.** X-band synthetic aperture radar applications for environmental monitoring. Tartu, 2014, 117 p.
92. **Deivid Pugal.** hp-FEM model of IPMC deformation. Tartu, 2014, 143 p.
93. **Siim Pikker.** Modification in the emission and spectral shape of photostable fluorophores by nanometallic structures. Tartu, 2014, 98 p.
94. **Mihkel Pajusalu**. Localized Photosynthetic Excitons. Tartu, 2014, 183 p.
95. **Taavi Vaikjärv.** Consideration of non-adiabaticity of the Pseudo-Jahn-Teller effect: contribution of phonons. Tartu, 2014, 129 p.
96. **Martin Vilbaste.** Uncertainty sources and analysis methods in realizing SI units of air humidity in Estonia. Tartu, 2014, 111 p.
97. **Mihkel Rähn.** Experimental nanophotonics: single-photon sources- and nanofiber-related studies. Tartu, 2015, 107 p.
98. **Raul Laasner.** Excited state dynamics under high excitation densities in tungstates. Tartu, 2015, 125 p.
99. **Andris Slavinskis.** EST Cube-1 attitude determination. Tartu, 2015, 104 p.
100. **Karlis Zalite**. Radar Remote Sensing for Monitoring Forest Floods and Agricultural Grasslands. Tartu, 2016, 124 p.
101. **Kaarel Piip.** Development of LIBS for *in-situ* study of ITER relevant materials. Tartu, 2016, 93 p.
102. **Kadri Isakar.** $^{210}$Pb in Estonian air: long term study of activity concentrations and origin of radioactive lead. Tartu, 2016, 107 p.
103. **Artur Tamm.** High entropy alloys: study of structural properties and irradiation response. Tartu, 2016, 115 p.
104. **Rasmus Talviste.** Atmospheric-pressure He plasma jet: effect of dielectric tube diameter. Tartu, 2016, 107 p.
105. **Andres Tiko.** Measurement of single top quark properties with the CMS detector. Tartu, 2016, 161 p.
106. **Aire Olesk.** Hemiboreal Forest Mapping with Interferometric Synthetic Aperture Radar. Tartu, 2016, 121 p.
107. **Fred Valk.** Nitrogen emission spectrum as a measure of electric field strength in low-temperature gas discharges. Tartu, 2016, 149 p.
108. **Manoop Chenchiliyan.** Nano-structural Constraints for the Picosecond Excitation Energy Migration and Trapping in Photosynthetic Membranes of Bacteria. Tartu, 2016, 115p.
109. **Lauri Kaldamäe.** Fermion mass and spin polarisation effects in top quark pair production and the decay of the higgs boson. Tartu, 2017, 104 p.
110. **Marek Oja.** Investigation of nano-size α- and transition alumina by means of VUV and cathodoluminescence spectroscopy. Tartu, 2017, 89 p.
111. **Viktoriia Levushkina.** Energy transfer processes in the solid solutions of complex oxides. Tartu, 2017, 101 p.
112. **Mikk Antsov.** Tribomechanical properties of individual 1D nanostructures: experimental measurements supported by finite element method simulations. Tartu, 2017, 101 p.

113. **Hardi Veermäe.** Dark matter with long range vector-mediated interactions. Tartu, 2017, 137 p.
114. **Aris Auzans.** Development of computational model for nuclear energy systems analysis: natural resources optimisation and radiological impact minimization. Tartu, 2018, 138 p.
115. **Aleksandr Gurev**. Coherent fluctuating nephelometry application in laboratory practice. Tartu, 2018, 150 p.
116. **Ardi Loot**. Enhanced spontaneous parametric downconversion in plasmonic and dielectric structures. Tartu, 2018, 164 p.
117. **Andreas Valdmann.** Generation and characterization of accelerating light pulses. Tartu, 2019, 85 p.
118. **Mikk Vahtrus.** Structure-dependent mechanical properties of individual one-dimensional metal-oxide nanostructures. Tartu, 2019, 110 p.
119. **Ott Vilson.** Transformation properties and invariants in scalar-tensor theories of gravity. Tartu, 2019, 183 p.
120. **Indrek Sünter.** Design and characterisation of subsystems and software for ESTCube-1 nanosatellite. Tartu, 2019, 195 p.
121. **Marko Eltermann**. Analysis of samarium doped $TiO_2$ optical and multiresponse oxygen sensing capabilities. Tartu, 2019, 113 p.
122. **Kalev Erme**. The effect of catalysts in plasma oxidation of nitrogen oxides. Tartu, 2019, 114 p.
123. **Sergey Koshkarev.** A phenomenological feasibility study of the possible impact of the intrinsic heavy quark (charm) mechanism on the production of doubly heavy mesons and baryons. Tartu, 2020, 134 p.
124. **Kristi Uudeberg.** Optical Water Type Guided Approach to Estimate Water Quality in Inland and Coastal Waters. Tartu, 2020, 222 p.
125. **Daniel Blixt.** Hamiltonian analysis of covariant teleparallel theories of gravity. Tartu, 2021, 142 p.
126. **Ulbossyn Ualikhanova.** Gravity theories based on torsion: theoretical and observational constraints. Tartu, 2021, 154 p.
127. **Iaroslav Iakubivskyi**. Nanospacecraft for Technology Demonstration and Science Missions. Tartu, 2021, 177 p.